THE ASTROPHYSICAL JOURNAL, 488:807–826, 1997 October 20
© 1997. The American Astronomical Society. All rights reserved. Printed in U.S.A.

# NONSPHERICAL STRUCTURES AND TEMPORAL VARIATIONS IN THE DUST SHELL OF o CETI OBSERVED WITH A LONG BASELINE INTERFEROMETER AT 11 MICRONS

B. LOPEZ,[1] W. C. DANCHI, M. BESTER, D. D. S. HALE,[2] E. A. LIPMAN, J. D. MONNIER, P. G. TUTHILL, AND C. H. TOWNES
Space Sciences Laboratory, University of California, Berkeley, Berkeley, CA 94720-7450
C. G. DEGIACOMI
KOSMA, I. Physikalisches Institut, Universität zu Köln, Zülpilcher Strasse, 77 D-50937 Köln, Germany
T. R. GEBALLE
United Kingdom Infrared Telescope, 660 North A'ohoku Place, University Park, Hilo, HI 96720
L. J. GREENHILL
Harvard-Smithsonian Center for Astrophysics, 60 Garden Street, Cambridge, MA 02138
P. CRUZALÈBES, J. LEFÈVRE AND D. MÉKARNIA
Observatoire de la Côte d'Azur, Department Fresnel, UMR 6528, BP 229 06304 Nice Cedex 4, France
J. A. MATTEI
American Association of Variable Star Observers, 25 Birch Street, Cambridge, MA 02138
D. NISHIMOTO
Rockwell Power Systems, 535 Lipoa Parkway, Suite 200, Kihei, HI 96753
AND
P. W. KERVIN
USAF Phillips Laboratory, Kihei, HI 96753
*Received 1996 October 7; accepted 1997 June 2*

## ABSTRACT

Visibility observations at 11 $\mu$m of o Ceti have been made with the University of California (Berkeley) Infrared Spatial Interferometer during the time period 1988–1995. The observed visibilities change dramatically from one epoch to another and are not consistent with simple heating or cooling of the dust with change in luminosity as a function of stellar phase. Instead, large temporal variations in the density of dust within a few stellar radii of the photosphere of o Ceti have occurred. Spherically symmetric models of the dust distribution with two dust shells, one within three stellar radii of the photosphere of the star, the other approximately 10 stellar radii from the star, can account reasonably well for the observed changes. Four types of axially symmetric radiative transfer models were also compared with the data—a spherical shell with an ellipsoidal inner cavity, a disk, a spherical shell with one or two inhomogeneities or clumps, and a set of thin partial shells with a fixed distance between them. Of the four models, only the one with the ellipsoidal inner cavity is excluded. The data were best-fitted with the last two models, which emphasize inhomogeneities or clumps. To fit the observed temporal changes in the visibility data, all models must include a change in the density—increasing and decreasing—of dust close to the photosphere of the star. The axially symmetric models had clumps placed at distances from the star in agreement with distances of the spherical models. Good fits to the observed broadband spectrum of the star were also obtained with these models.

*Subject headings:* circumstellar matter — infrared: stars — stars: individual (o Ceti) — stars: mass loss — stars: variables: long-period variables — techniques: interferometric

## 1. INTRODUCTION

Long-period variable stars represent a relatively short but significant portion of the lifetime of many stars. During this phase typical stars may lose enough mass to the interstellar medium to prevent them from becoming supernovae (Iben 1985, 1991). The resulting circumstellar envelopes contain dust and molecules and have been studied by a variety of methods and across a large part of the electromagnetic spectrum during the past few decades.

Millimeter and submillimeter wave emission lines from rotational transitions of carbon monoxide and other molecules have been the dominant tools in detailed studies of the envelopes of these stars. The spatial distributions, mass-loss rates, and physical conditions in these shells have been examined at angular scales ranging from tens of arcsec to a few arcminutes (Knapp & Morris 1985; Sahai & Beiging 1993; Young 1995).

The connection between large-scale outflows and phenomena occurring at or near the photospheres of these stars, such as pulsation and convection, is not well understood, although there are a number of theoretical models that can provide such a connection (see Bowen 1988; Hearn 1990, p. 121; Winters et al. 1995). Detailed observations at a variety of wavelengths and at very high spatial resolution, comparable to the dimensions of the stars themselves, are required for further progress in this area. For example, at centimeter and millimeter wavelengths, such observations have been

[1] Observatoire de la Côte d'Azur, Department Fresnel, UMR 6528, BP 229 06304 Nice Cedex 4, France.
[2] Allegheny Observatory, University of Pittsburgh.

made with the Very Long Baseline Array utilizing maser emission from SiO molecules as a tracer of material close to the star (e.g., Greenhill et al. 1995; Diamond et al. 1994).

At near-infrared and optical wavelengths high-resolution work has been focussed on measurements of diameters of a number of these stars using the tools of speckle interferometry (Karovska et al. 1991; Karovska, Nisenson, & Beletic 1993), nonredundant aperture masking (Haniff et al. 1992; Wilson et al. 1992; Tuthill 1994; Tuthill, Haniff, & Baldwin 1995), and long baseline interferometry (Quirrenbach et al. 1992).

At mid-infrared wavelengths, most studies have used low-resolution spectra of the silicate emission features to determine the physical conditions and distribution of the dust, albeit indirectly through modeling (e.g., David & Papoular 1992; van der Veen et al. 1995). In addition, there has been a modest amount of direct imaging work with resolutions typically of about an arcsec (see Bloemhof et al. 1984; Danchi et al. 1992; Meixner 1993).

Long baseline interferometry in the mid-infrared has progressed to the point where significant observational studies of long-period variable stars have been published. A review of instrumentation and results of long baseline stellar interferometry at optical and infrared wavelengths was published recently by Danchi & Bester (1995). Results have been obtained both in survey and monitoring modes, for example, a survey of 13 such stars was recently published (see Danchi et al. 1994a). The longer term studies have focussed on prototypical cases of classes of such stars, namely the bright oxygen-rich supergiant $\alpha$ Orionis (Bester et al. 1996), the bright carbon star IRC +10216 (Danchi et al. 1990, 1994a), and on o Ceti or Mira itself (Bester et al. 1991; Danchi et al. 1994a).

In the present paper visibility data from o Ceti taken from 1988 to 1995 are analyzed and interpreted using both spherically symmetric and axially symmetric radiative transfer models. Substantial variations in the 11 $\mu$m visibility have been observed that cannot be interpreted as being due only to changes in the luminosity of the star with phase. Instead, substantial variations in the density of dust close to the photosphere are required by all models to explain the observed variations. Additionally, all models characteristically involve departure from a simple uniform mass loss, in the form of multiple discrete shells, disks, or clumps. Recent observations of variations in the visible and 10 $\mu$m wavelength luminosities, and of the spectrum of o Cet in the 10 $\mu$m region are also included and discussed in terms of these models.

The remainder of this paper is organized into a section on observations, followed by a comparison with other observations. Detailed discussions of the modeling are in sections on spherical models, spherical dust shells with aspherical inner cavities, disk models, and clump models. The paper ends with a discussion of the results and future directions of work.

## 2. OBSERVATIONS

### 2.1. *Visibility Measurements*

Visibility observations for the long-period variable o Ceti have been obtained over the past seven years with the U. C. Berkeley Infrared Spatial Interferometer (ISI). The ISI currently is a two-element interferometer comprised of movable 1.65 m aperture telescopes, with Pfund-type optics and heterodyne detection. The present site layout allows for baselines between 4 and 35 m with a variety of orientations (see Bester, Danchi, & Townes 1990; Bester et al. 1992). The observations with the ISI discussed here have been obtained at a wavelength of 11.15 $\mu$m, although observations at other discrete wavelengths in the 9–12 $\mu$m atmospheric window are possible with the present instrumentation.

The visibility observations provide direct information on the spatial distribution of dust emission at spatial scales as small as 32 milliarcseconds (mas). Visibility data and corresponding model curves for maximum and minimum luminosity phases for epochs to 1992 have been published in papers by Bester et al. (1991), Degiacomi et al. (1992), and Danchi et al. (1994a, 1994b). Observations were made with baselines as small as 4 m and as large as 32 m. Visibilities were calibrated relative to $\alpha$ Tau, a K5 giant having no dust emission.

The interpretation of the visibility data was based on a spherical radiative transfer model (see Danchi et al. 1994a). The density distribution for the dust used in most models was proportional to $r^{-2}$, where $r$ denotes the radial distance from the center of the star. Physically, this density distribution corresponds to a constant outflow of dust particles in a dust shell expanding at a constant velocity. Alternative models were also explored that included an enhancement in the density of dust at the inner edge of the dust shell due to acceleration of dust by radiation pressure. The main result of these studies were estimates of the inner radius of the dust shell, the temperature of the hot dust at the inner edge, the optical depth of the envelope, and the stellar temperature and diameter. An overview of parameters obtained from these models is presented in Table 1.

Substantial variations are noted in the visibility curves obtained from 1988 to 1992. This set of visibilities is displayed in chronological order in Figure 1. Variations appear not only during changes related to the phase of the luminosity cycle of o Ceti but also from cycle to cycle.

Bester et al. (1991) and Degiacomi et al. (1992) modeled o Ceti and its surrounding dust shell as a function of the luminosity cycle ($P \sim 331$ days), shown here in Figure 1*a*. The modeling of both the visibility curve of 1989 maximum and 1990 minimum ("Model 1" and "Min 1" in Table 1) shows that dust formation around o Ceti was well suited to account for the observed change in the visibility. Since the inner radius of the dust shell went from 0.″03 during minimum luminosity to 0.″05 during maximum luminosity, some additional dust was formed during the phase of minimum luminosity of the source. The 1990 minimum is poorly fitted by the model, particularly at the lowest spatial frequencies, because the visibilities fall much more quickly with increasing spatial frequency than is indicated by the $r^{-2}$ density law used in these models. Inhomogeneities in the density distribution could also affect the visibilities in a similar way.

The new visibility data taken in 1992 shows that the above interpretation of earlier data clearly does not give a correct picture of the dust formation around o Ceti. Indeed, an important difference appears between the ISI data obtained from 1989 October 10 to December 5 ($\phi = 0.94$–$0.11$) and with the 1992 data from July 15 to August 15 ($\phi = 0.98$–$0.08$). For the two sets of data, the luminosity phase of the objects was essentially the same but separated by two cycles. From cycle to cycle the object was presenting some unexpected changes as discussed in Danchi et al.

TABLE 1

PRIOR MODELS OF o CETI

| Observation Dates | Model Name | $R_*$[d] (mas) | $T_*$[e] (K) | $R_0$[f] (mas) | $T_0$[g] (K) | $\tau_{11}$[h] | $F_{11}$[i] (Jy) |
|---|---|---|---|---|---|---|---|
| 1989 ..... | Model 1[a] | 16.8 | 2850 | 50 | 1170 | 1.067 | 4520 |
| 1989–1990 ..... | Max L1[b] | 17.0 | 2850 | 50 | 1170 | 0.087 | 4210 |
| | Min L1 | 17.0 | 2270 | 30 | 1208 | 0.080 | 2750 |
| 1992 ..... | Max 1[c] | 19.3 | 2700 | 50 | 1344 | 0.10 | 4200 |
| | Max 2 | 19.3 | 2700 | 60 | 1276 | 0.14 | 5000 |
| | Min 1 | 23.6 | 2200 | 60 | 1063 | 0.17 | 3731 |

[a] "Model 1" of Bester et al. 1991 is labeled as "Model 1" in Fig. 1*a*.
[b] "Min 1" of Danchi et al. 1994b is labeled as "Model for 1990" in Fig. 1*b*.
[c] "Max 1 & Max 2" of Danchi et al. 1994b are labeled by "Model 1 & Model 2" in Fig. 1*c*.
[d] Photospheric angular radius.
[e] Effective temperature.
[f] Inner radius of dust shell.
[g] Temperature of dust at the inner radius.
[h] Optical depth at 11 $\mu$m from model.
[i] Flux density at 11 $\mu$m from model.

(1994a): the 1992 visibility measurement at maximum luminosity is apparently consistent with an enhanced density of dust closer to the star than it was previously during the 1989 maximum.

Additional visibility measurements were taken during the 1993 observing season (Danchi et al. 1994b) and more recently during the summer and early fall of 1994, and fall of 1995. The baseline was varied from 4 to 32 meters for this set of measurements (see Table 2 for a detailed journal of observations). No changes were noted between the visibility curves of 1993 taken approximately at maximum light and the one of 1994 observed at a similar phase one cycle later. Visibilities for 1993 and 1994 combined together are presented in Figure 2. A wide range of spatial frequencies has been covered (from $1.5 \times 10^5$ rad$^{-1}$ to $\sim 30 \times 10^5$ rad$^{-1}$), making the resulting visibility curve of o Ceti one of the most complete obtained up to now.

A qualitative comparison with the previous visibilities leads to the following remarks:

1. The newly measured visibilities show a bump at a spatial frequency of approximately $7 \times 10^5$ rad$^{-1}$. It is interesting to note that this bump was apparently also encountered in the shape of the 1990 visibility obtained during a minimum light of o Ceti.

2. The visibility curves at the luminosity maxima of 1993 and 1994 are consistent with the one observed in 1989. They also bring some new and more decisive information as the spatial frequencies explored in the Fourier ($u$, $v$) plane (see Fig. 3) overlap with the Fourier ($u$, $v$) track obtained in 1992.

3. The visibility data measured in 1992 differ from the rest of the data. Some asymmetries in the envelope might have produced the apparent variations observed between 1989 and 1992 because the baseline length and orientation for these two observing periods was quite different (see Fig. 3 and Table 2). Now that the observed changes in visibility in 1992 have been confirmed in a region where the spatial frequencies overlap with the data of 1993–1994, it is also noteworthy that an unusual event occurred in 1992 in the environment of o Ceti, as indicated by the unusually bright visible maximum seen in Figure 4.

### 2.2. *Photometry*

Long-term observations of the visual brightness of Mira show that the amplitude of its light curve variations can

TABLE 2

JOURNAL OF ISI OBSERVATIONS OF o CETI FROM 1988 TO 1995

| Dates | Nights | Phase[a] $\phi$ | Baseline (m) | Orientation |
|---|---|---|---|---|
| 1995 Oct 27, Nov 8, 9..... | 3 | 0.59 | 4 | N 89°.4 E |
| 1994 Sep 7–Oct 27 ..... | 13 | 0.34–0.50 | 4 | N 89°.4 E |
| 1994 Jul 27–Aug 19 ..... | 8 | 0.22–0.29 | 32 | N 118°.4 E |
| 1994 Jun 10–Jul 13 ..... | 6 | 0.08–0.18 | 32 | N 118°.4 E |
| 1993 Nov 6..... | 1 | 0.43 | 32 | N 118°.4 E |
| 1993 Aug 28–Sep 30..... | 7 | 0.21–0.31 | 9.6 | N 122°.7 E |
| 1993 Jul 26–Aug 21 ..... | 13 | 0.12–0.19 | 9.6 | N 122°.7 E |
| 1992 Jul 15–Aug 15 ..... | | 0.98–0.08 | 9.6 | N 122°.7 E |
| 1990 Jul 5–6 ..... | 2 | 0.75 | 13 | N 113° E |
| 1989 Dec 5 ..... | 1 | 0.11 | 13 | N 113° E |
| 1989 Nov 9,15 ..... | 2 | 0.03–0.06 | 13 | N 113° E |
| 1989 Oct 8,12 ..... | 2 | 0.94–0.95 | 4 | N 89° E |

[a] Phases are calculated relative to the visible maximum on JD 2448493 using a period of 331.9 days.

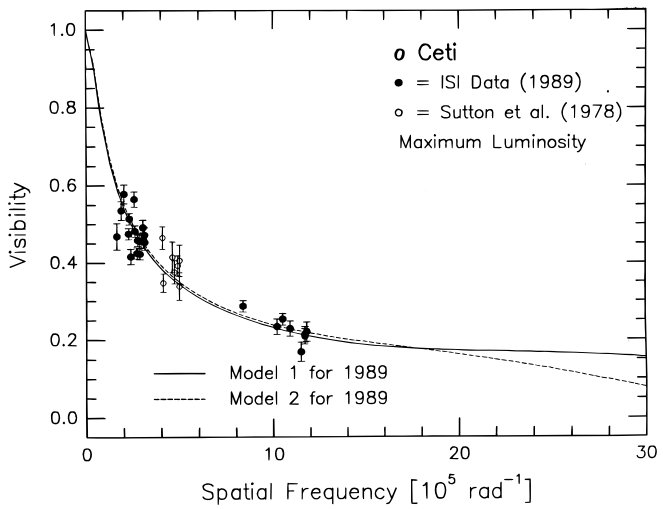


FIG. 1*a*

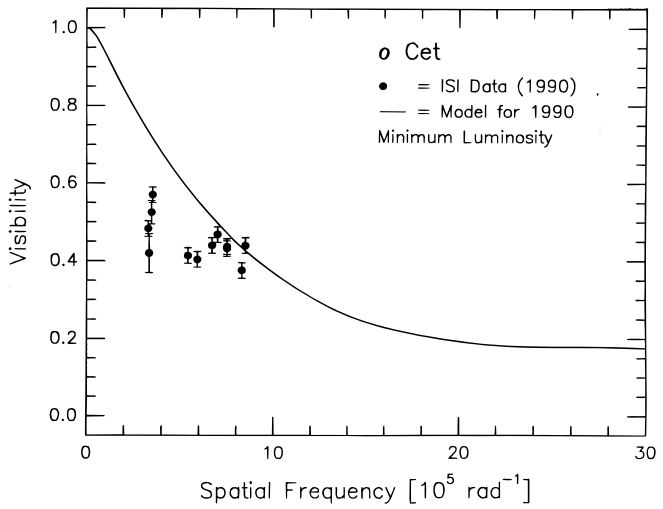


FIG. 1*b*

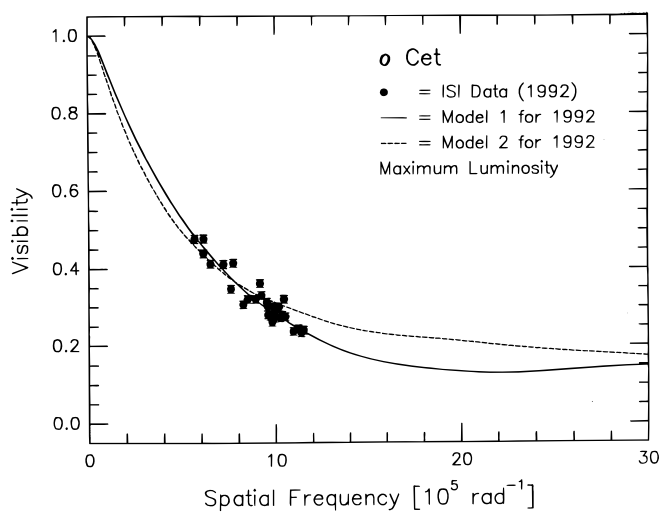


FIG. 1*c*

FIG. 1.—(*a*) Visibility data and model curve for o Ceti during luminosity maxima in 1989 and 1978 (after Bester et al. 1991). (*b*) Visibility data and model curve for o Ceti for the 1990 minimum (after Danchi et al. 1994a); (*c*) Visibility data and model curve for o Ceti for the 1992 maximum (after Danchi et al. 1994a). Note the substantial difference in visibility at $6 \times 10^5$ rad$^{-1}$ between this maximum and the 1989 maximum.

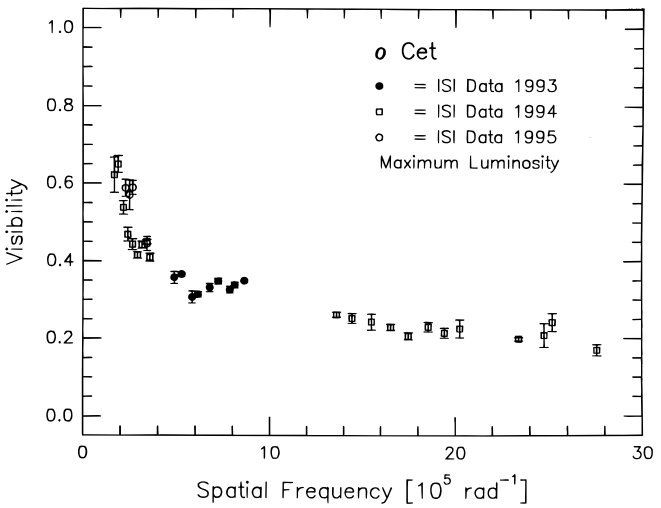


FIG. 2.—Visibility data and measurements for 1993 and 1994. Most of these data were taken near maximum luminosity. Note the substantial difference in visibilities between these data and those from the 1992 maximum, and the similarity to the data taken at the 1989 maximum.

change substantially from one cycle to another. Changes in the stellar luminosity may affect the surrounding environment and produce new dust or destroy existing dust. Figure 4*a* shows the curve of visual magnitude as reported by the members of AAVSO (American Association of Variable Star Observers) and AFOEV (Association Française des Observateurs d'Etoiles Variables). The solid curve is the best-fitting sinusoid for the time period JD 2445000 to JD 2448500. All the parameters for the sinusoid, i.e., the period, phase, amplitude, and offset, were fitted simultaneously by minimizing the $\chi^2$ using Powell's method (see Press et al. 1992, chap. 10, p. 412). The resulting values are 334.0 days for the period, 5.4 for the peak-to-peak amplitude, and 6.7 for the mean magnitude. The errors in the parameter esti-

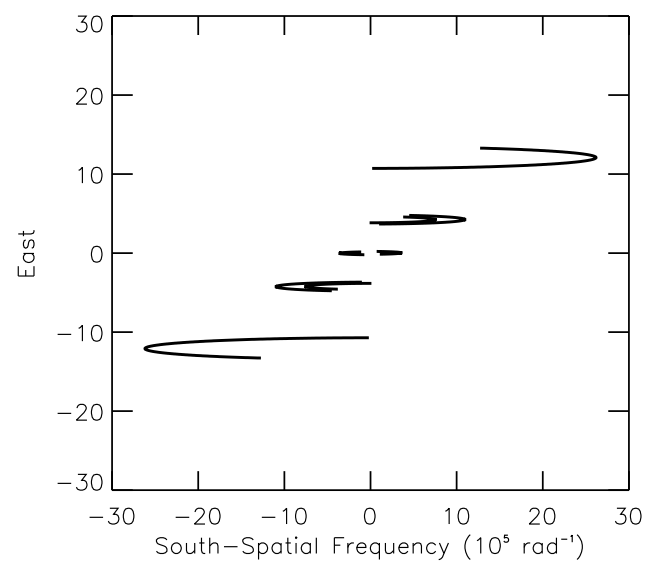


FIG. 3.—Fourier (*u*, *v*) plane coverage of the ISI for the various baselines used in this paper. Starting with the (*u*, *v*) track nearest the origin, the tracks can be identified with the individual baselines that were used for the observations. The innermost track corresponds to the 4 m baseline; the two tracks nearly overlapping correspond to the 9.6 and 13 m baselines; and the track furthest from the origin corresponds to the 32 m baseline.

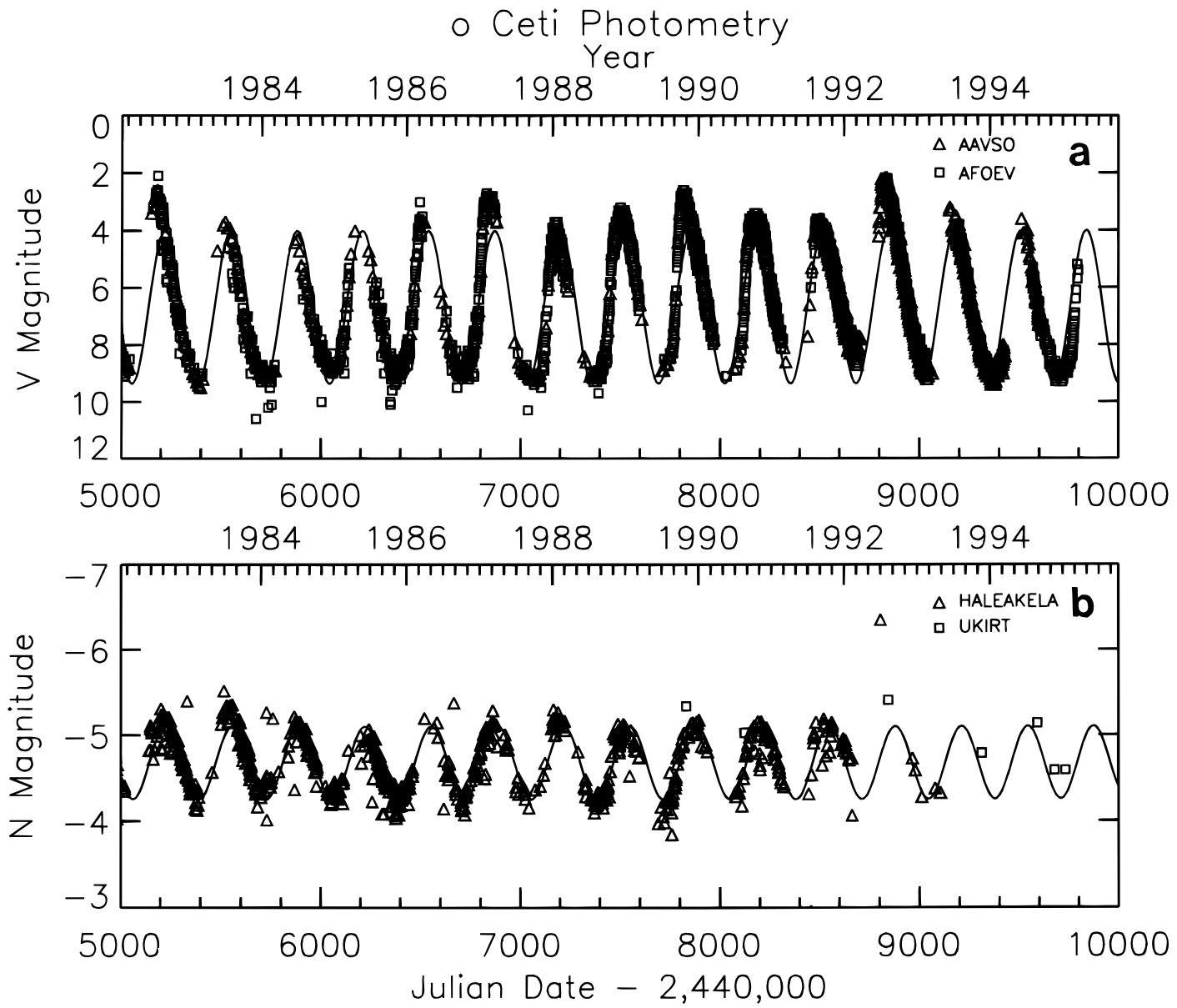


FIG. 4.—(*a*) Light curves for o Ceti from the American Association of Variable Star Observers (AAVSO) (*triangles*) and the (AFOEV) (*squares*). Note the excellent agreement between two sets of observers, the unusually bright maximum in 1992, and the unusually deep minima in subsequent years. (*b*) Photometry for *N* band from Haleakela (*triangles*) and from UKIRT (*squares*) for the same time period as the visible photometry.

mates are approximately 4 days, 0.4, and 0.2, for the period, peak-to-peak, and mean magnitude, respectively.

Note that the phase of the observations could also be determined from the interval between successive optical maxima. However, the period does vary substantially from cycle to cycle, which affects the estimate of the phase. For example, from 1988 to 1994 o Ceti went through seven cycles. The minimum period was 306 days, while the maximum was 353 days. The mean period was 331.9 days with probable error of 5.7 days. Since the estimate of the mean period in this paper is consistent with the usual one of 331.9 days, we adopt the latter period when estimating the phase for the observations reported here. All phases are calculated relative to the optical maximum on JD 2448493. The maximum variation between estimates of phase, either by measuring from cycle to cycle, or using the mean period, is approximately 0.05 and does not affect any of the conclusions in the paper.

The visible magnitude of the star during the maximum light in 1992 appears to be much brighter than that of the surrounding maxima (more than one magnitude of difference). While any direct interpretation is difficult to give, the brightness in visible light in 1992 is correlated with the observed variation in the 1992 visibility curve at 11.15 $\mu$m. The first visual monitoring of the magnitude of Mira is reported in 1835 by AAVSO members. Since then, several maxima as bright as the one of 1992 have occurred. Apparently, there is no regular period for this occurrence; however, typically the larger variations take place every 3–5 cycles. Another peculiar maximum occurred previously in 1989! It was not as bright by half a magnitude as the one of 1992 and apparently did not substantially affect the visibility data.

Figure 4*b* displays mid-infrared photometry from the Maui Space Surveillance Site (MSSS) (see Nishimoto et al. 1995) (*triangles*) and from the United Kingdom Infrared

Telescope (UKIRT) (*squares*), respectively. The MSSS observed a number of late-type stars on a nightly basis from 1980 to 1992 as part of the calibration of their infrared radiometer system. The MSSS radiometer consisted of a square array of 25 cadmium-doped germanium (Ge:Cd) photoconductive detectors, cooled to 12 K, and installed on the 1.2 m telescope. The telescope secondary was chopped at 50 Hz, and the chopped signal was recorded with a filter time constant of 0.3 s. Typically, an *N*-band equivalent filter was used for the observations. The MSSS operates under a broader range of atmospheric conditions than would be acceptable for normal astronomical observatory; because of that and the limited integration time, the peak-to-peak variation of the observations is approximately 0.4 mag at *N* band for most of the observations, but it could be even greater under some conditions. As with the optical data, the mid-infrared photometry data were fitted for the parameters of the sinusoid. In this case the period was 332.0 days, amplitude (peak-to-peak) was 0.8, and the mean magnitude was $-4.7$ for the *N* band. The errors in these fitted values are similar to those for the optical data. The maximum of the sinusoidal fit to the optical data leads that of the mid-infrared by approximately 46 days. The actual optical maxima lead the mid-infrared maxima by a total of 77 days since the actual optical maxima occur approximately 31 days prior to the maxima of the fitted sinusoid. The infrared lag observed in this work is consistent with the approximately 0.1 period lag between optical and near-infrared maxima noted by Lockwood & Wing (1971).

The contribution of photospheric temperature and size variations to the 10 $\mu$m variation is small. A simple calculation yields the variation of 0.3 mag at 10 $\mu$m if there is a 500 K temperature variation in photospheric temperature, keeping the stellar radius constant. The mid-infrared variation is smaller if the estimates of stellar radius and temperature from Table 4 (see below) are used. In this case the variation is 0.15 mag. Thus, the main contribution to the variability at 10 $\mu$m is due to temperature and opacity variations in the dust shell rather than the star itself.

Measurements of the mid-infrared luminosity were made at UKIRT from 1989 to the present. Both narrowband photometry (using the single channel bolometer in UKT8) and more recently 7–13 $\mu$m spectrophotometry (using the linear array spectrometer CGS3) have been employed, using 5″ diameter apertures and standard chopping and nodding techniques. Flux calibrations, derived from observations of $\alpha$ Lyrae, $\alpha$ Aurigae, and $\alpha$ CMa, are believed to be accurate to approximately 3% for all observations reported here. Wavelength calibration of the spectra was derived from the line emission of a krypton arc lamp observed in fourth, fifth, and sixth order. The spectra of o Ceti, shown here in Figure 5, are dominated by strong absorption due to photospheric SiO at 7–9 $\mu$m and emission due to circumstellar dust particles at 9–12 $\mu$m. Details of the shape of the spectra are least reliable near the peak of the silicate emission at 9.7 $\mu$m, due to the strong telluric absorption by ozone of radiation near that wavelength. The flux densities at 11.15 $\mu$m are listed in Table 3.

In the next section, we will discuss other relevant information that may help in understanding what might be responsible for the observed variations in the environment of Mira. Several questions arise: can evaporation or formation of new dust account for such observed changes; what may be the effects of asymmetries in the envelope of Mira; do hot spots on the star and clumpiness in the shell also modify the radiative transfer in the dust shell?

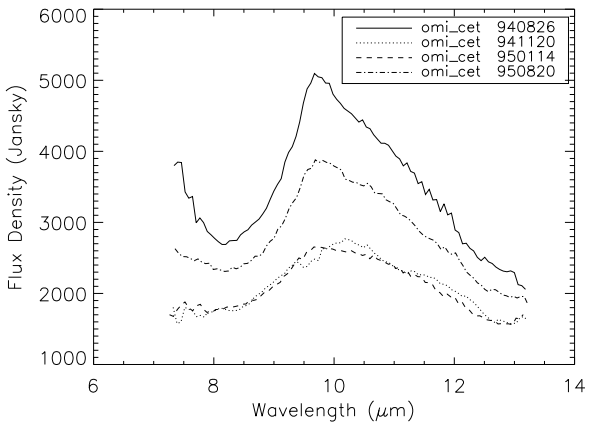


FIG. 5.—Mid-infrared spectra of o Ceti taken with CGS3 at the United Kingdom Infrared Telescope (UKIRT). Note the substantial variation in flux density for 1994–1995.

In a later section, new dust shell models for the 1993–1994 visibility curves are presented. According to these models, variations in the dust near the star are shown to be an appropriate explanation for the peculiar visibility of 1992.

## 3. COMPARISON WITH OTHER OBSERVATIONS

Asymmetries in the shape of Mira or its dust shell may also play an important role in the variation of the observed visibilities. The presence of concentrations of dust or clumps and the way they are illuminated by stellar light can affect the observable properties of the object. A number of observations have shown some evidence for asymmetries at the stellar scale and also at larger scales in the surrounding envelope (Karovska et al. 1991; Wilson et al. 1992; Planesas, Kenney, & Bachiller 1990; Haniff et al. 1992; Quirrenbach et al. 1992; Tuthill 1994).

At optical wavelengths near 0.7 $\mu$m, the shape of Mira itself is elongated, with an axial ratio of 0.85 and major axis at a position angle of about 120°. Karovska et al. (1991) fitted uniform ellipses to power spectra derived from speckle images and found a major axis of 68 mas, axial ratio of 0.85, and position angle of 115°. Wilson et al. (1992) fitted Gaussian ellipses to their visibility curves and obtained about 30 mas for the major axis, axial ratio of 0.85 and a position

TABLE 3

JOURNAL OF UKIRT OBSERVATIONS OF o CETI FROM 1989 TO 1995 AT 11.15 MICRONS

| Dates | Phase[a] $\phi$ | Flux Density[b] (Jy) |
|---|---|---|
| 1989 Nov 1 ..... | 0.03 | 4550 |
| 1990 Aug 11 ..... | 0.86 | 3490 |
| 1992 Aug 19 ..... | 0.09 | 4850 |
| 1993 Nov 20..... | 0.47 | 2750 |
| 1994 Aug 26 ..... | 0.31 | 3800 |
| 1994 Nov 20..... | 0.58 | 2300 |
| 1995 Jan 14..... | 0.73 | 2290 |
| 1995 Aug 20 ..... | 0.39 | 3100 |

[a] Phases are calculated relative to the optical maximum on JD 2448493 using a period of 331.9 days.

[b] Error in measured flux density approximately 3%.

angle of 120°. Haniff et al. (1992) also fitted uniform ellipses and obtained a major axis of 55 mas, axial ratio of 0.82, and position angle of 119°. A three component model with a large component was employed by Quirrenbach et al. (1992). The largest component has a major axis of length 68 mas, axial ratio of 0.86, and position angle of 86°, containing 39% of the flux. The middle-sized, smaller component has a major axis of 33 mas, axial ratio of 0.69, and position angle of 121° with 47% of the flux. The third, or smallest and unresolved component contains 14% of the flux.

Although the shape of the star itself was mostly considered to explain its apparent elongation, two alternative interpretations are also possible: the presence of hot spots on the stellar photosphere or radiative transfer effects related to scattering in the asymmetries of the dust shell.

The presence of some hot spots on the stellar photosphere may modify the spatial power spectrum of the star in a similar manner as stellar elongation does. The study of Tuthill (1994), in which hot spots on Mira's atmosphere were observed using aperture masking techniques, shows that the phase of the object's Fourier transform must be recovered to distinguish between stellar elongation and the presence of hot spots. Different photospheric disk models containing from one up to three bright features were needed to explain the data observed at three different epochs. It was demonstrated that the nonsymmetric models (disk plus spots) were more appropriate than symmetric elliptical models to fit both power spectrum and phase information.

The scattering from higher density regions of dust may also strongly modify the apparent shape of the star. It is reasonable to think that the spatial distribution of dust is not homogeneous. At large spatial scales, from CO ($J = 2$–1) maps, Planesas et al. (1990) found evidence for asymmetries in the extended envelope of gas surrounding Mira. The CO maps at 6″ resolution show two lobes of gas, a blueshifted one approximately 3″ north of the stellar position and a redshifted emission observed to the south. The measurements are interpreted as representing a very slow bipolar outflow due to a partial collimation of the wind by higher density gas in the equatorial plane of the inner part of the molecular envelope.

Finally, it is interesting to note that the stellar atmosphere appears to be asymmetrical as traced by TiO emission in the TiO minus continuum map (Haniff et al. 1992). The TiO emission lies in an arc of mean position angle 113° and at approximately 35 mas from the center of the star. There is also a smaller knot at position angle 320°. The mean position angle of the main arc is very close to the position angle of the companion star, Mira B. It was noted by Danchi et al. (1994a) that the dust was nucleating at the same location (considering only the radial distance from the star) as the arc. Several interpretations may explain the aspherical TiO map: EUV radiation from Mira B preferentially illuminating one side of Mira atmosphere and causing scattering and/or fluorescence (Danchi el al. 1994a), asymmetries in the outer atmosphere of Mira as traced by the TiO, or modification of the radiative transfer of light due to nonhomogeneous dust distribution.

## 4. SPHERICAL MODELS

The very large changes in the observed visibility data taken between 1989 and 1994 are difficult to explain with the simplest possible spherical model, that of a single continuous dust shell beginning at an inner radius $R_0$ and a power-law density distribution. Previously published models accounted for the changes shown in Figures 1 and 2 as either due to a change in the inner radius or a change in the stellar luminosity. However, it is difficult for a single such model to account for the observed data as can be seen in Figures 10*a* and 12*a* of Danchi et al. (1994a), where the best-fitting maximum luminosity model for the 1992 maximum data did not fit the 1990 minimum luminosity data very well at all, particularly for spatial frequencies below $7 \times 10^5$ rad$^{-1}$. The model visibility curve was always significantly higher than the data, indicating the model had much more dust emission close to the star in the 1992 maximum compared to the 1990 minimum. However, the visibility data for the 1989 and 1993–1994 data lie well below the 1992 data for similar luminosity phases, indicating much more emission from dust close to the star at the 1992 maximum compared to any time either before or after that maximum.

The spherical models used in this paper are based on a radiative transfer code adapted from the work of Wolfire & Cassinelli (1986). A detailed discussion of the modeling code and procedures is presented in Danchi et al. (1994a) and will be only briefly discussed here. The radial temperature distribution of the dust is computed self-consistently assuming the star is a blackbody with an effective temperature, $T_*$, and radius, $R_*$. The dust has an inner radius, $R_0$, outer radius, $R_1$, and power-law density distribution. If more than one shell is used then each shell is similarly parameterized. The optical constants of the dust are from Draine & Lee (1984, 1987), and the grains are assumed to have a power-law size distribution. For a grain radius, $a$, the number density of grains having that radius, $n(a)$, is given by $n(a) \sim a^{-3.5}$, with $0.005 \leq a \leq 0.25$ $\mu$m (Mathis, Rumpl, & Nordseick 1977). The transfer code is performed at 47 wavelengths from the Lyman edge to 1000 $\mu$m and computes the specific intensity as a function of the distance from the center of the star and also the broadband spectrum.

The simplest spherically symmetric model that can account for the data uses two spherical shells, one with an inner radius close to the star, i.e., within a few $R_*$, followed by a steep falloff in density, until there is a second dust shell, beginning much further from the star, i.e., $\sim 10R_*$, as can be seen in the schematic illustration of Figure 6. Calculated visibilities for a model that accounts reasonably well for the behavior of the data are displayed in Figure 7, and the parameters are given in Table 4. This model was constructed by deriving the optimum parameters for the most recent 1993–1994 data (cf. Fig. 7*c*). The best fit for the 1992 maximum is obtained by increasing the density of dust in the innermost shell and is shown in Figure 7*b*. This required an increase in density by a factor of 3.5, which increased the total optical depth by almost a factor of 2, as can be seen in Table 4. The 1990 minimum is obtained from the model of Figure 7*b* by decreasing the density of dust in the innermost shell compared to that of the original model for the 1993–1994 data, and by decreasing the stellar luminosity by a factor of 2. The fit of this model to observations during the 1990 minimum is shown in Figure 7*a*. Visibility data for the 1989 maximum agree well with the 1993–1994 data taken over the same spatial frequency; hence it is not necessary to separately model these data, since the model accounts for the latter data very well.

Clearly, the more complicated two-shell model better describes the totality of visibility data than does a simple

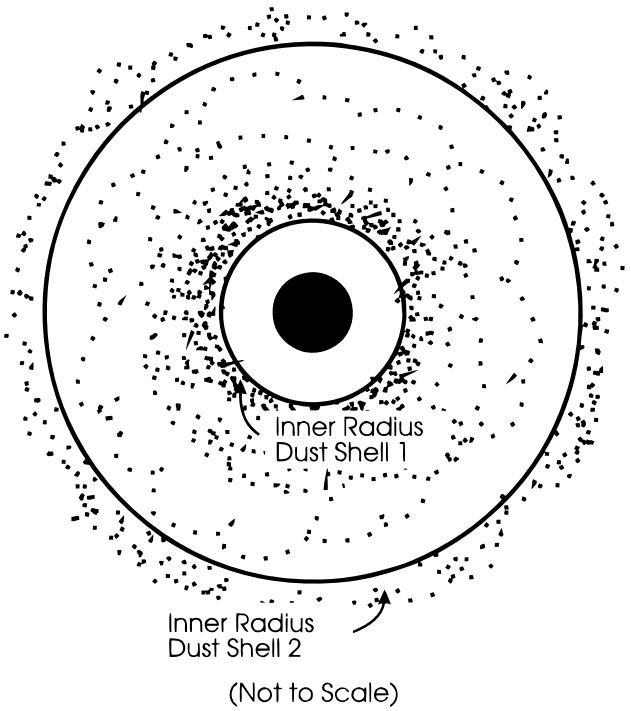


FIG. 6.—Schematic illustration of a dust model for o Ceti, consisting of two dust shells, one close to the star ($\sim 50$ mas or $\sim 3\,R_*$), the other much further away ($\sim 200$ mas or $12\,R_*$).

single shell model, even with a change in the inner radius. This occurs because the presence of the dust in the inner shell enhances the changes in 11 $\mu$m brightness close to the star and relative to the dust further out, which is itself in the region where the Planck function $B_\nu(T)$ is exponentially sensitive to the temperature of the dust. A still better quality of fit for o Ceti occurs with models that are axially symmetric rather than spherically symmetric.

## 5. ASYMMETRICAL MODELS—GENERAL DEVELOPMENT

The models employed hereafter assume the envelope geometry departs from spherical symmetry. However, one symmetry axis is retained in the analysis of the visibility curves. The numerical simulation of the radiative transfer in an axisymmetric dust cloud is based on a Monte Carlo method. This method has been often used in the case of spherical geometry (see, e.g., Lefèvre, Bergeat, & Daniel 1982). Details of the numerical simulation for axisymmetric geometry used in this paper are given in Lopez et al. (1994).

The numerical simulation is used to solve the problem of the radiative transfer through the dust shell and to compute the radiative equilibrium of dust grains. The star in the model is assumed to radiate as a blackbody and is characterized by its effective temperature $T_*$. The spatial dust grain distribution is an axisymmetric function bounded by an inner and outer limits denoted by $R_0$ and $R_1$, respectively. The radial distance from the center of the star is normalized to photospheric radius units. The dust grains are assumed to be of homogeneous composition and spherical with radius $a$. The Mie theory is used to calculate the optical constants of dust particles: $Q_{\rm ext}$ (the extinction efficiency), $Q_{\rm abs}$ (the absorption efficiency), $Q_{\rm sca}$ (the scattering efficiency), and $S(\theta)$ (the scattering diagram) giving the angular dependence of the scattered radiation.

The complex dielectric constants of the silicate presently used for the study of the dust envelope of o Ceti were taken from Draine & Lee (1984).

In the Monte Carlo method used, stellar radiation and thermal emission from dust particles are generated by a set of radiation trajectories. Thirty wavelengths are used to represent the emergent spectrum from the star and the emergent spectrum from dust particles.

At the beginning of the algorithm, radiation is first emitted by the star. The direction of initial propagation of the radiation is chosen randomly. The length $l$ of the effective radiation trajectory from the origin of emission up to the interaction with a grain of the dusty envelope is chosen randomly. The density probability of the random process is proportional to $\exp[-\tau(l)]$, where $\tau(l)$ is the optical depth along the direction of propagation. For each interaction, a fraction of the radiation leaves the envelope, a fraction is absorbed and a fraction is scattered. The direction of scattering is randomly chosen according to the scattering diagram. The scattered fraction of the radiation continues then to propagate in the three-dimensional dusty medium. Several interactions between the radiation and the grains will successively occur. Each time the energy of the scattered radiation becomes lower. After most of its initial energy is lost from multiple scattering, the propagating radiation is neglected. New radiation is then generated from the star and later in the process from thermally emitting dust particles.

The radiative equilibrium of the dust particle, which depends on both the stellar radiation and the grain-grain radiative exchanges, is determined in a self-consistent way. In the present simulation the dust shell is sampled in about 400 isothermal tori. Radiative exchanges between the star and tori and between each torus and another constrain the

TABLE 4

SPHERICAL MODEL PARAMETERS

| Epoch | $R_*$ (mas) | $T_*$ (K) | Shell Number | $R_0$ (mas) | $T_0$ (K) | $\alpha$[a] | $\tau_{11}$[b] |
|---|---|---|---|---|---|---|---|
| Epoch 1..... | 23.6 | 2200 | Shell 1 | 50 | 1164 | 3.50 | 0.036 |
| (1990) ..... | | | Shell 2 | 200 | 600 | 1.50 | 0.059 |
| Epoch 2..... | 19.3 | 2700 | Shell 1 | 50 | 1380 | 3.50 | 0.127 |
| (1992) ..... | | | Shell 2 | 200 | 600 | 1.50 | 0.059 |
| Epoch 3..... | 19.3 | 2700 | Shell 1 | 50 | 1340 | 3.50 | 0.036 |
| (1993–1994)..... | | | Shell 2 | 200 | 600 | 1.50 | 0.059 |

[a] Power law for radial density distribution, i.e., $n(r) \sim r^{-\alpha}$.
[b] Optical depth at 11 $\mu$m.

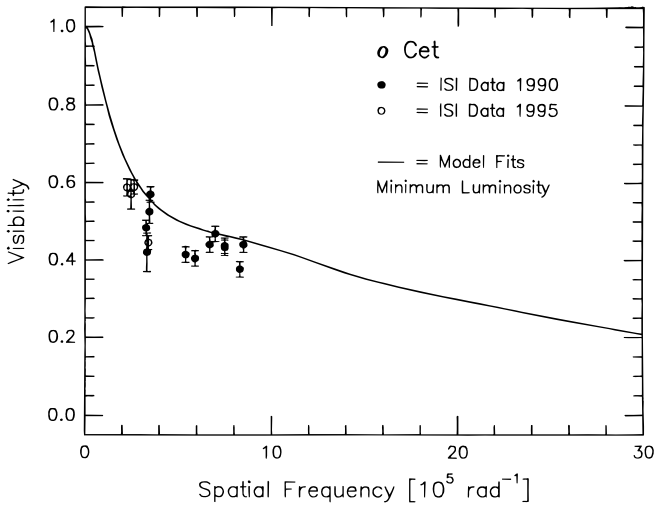


FIG. 7a

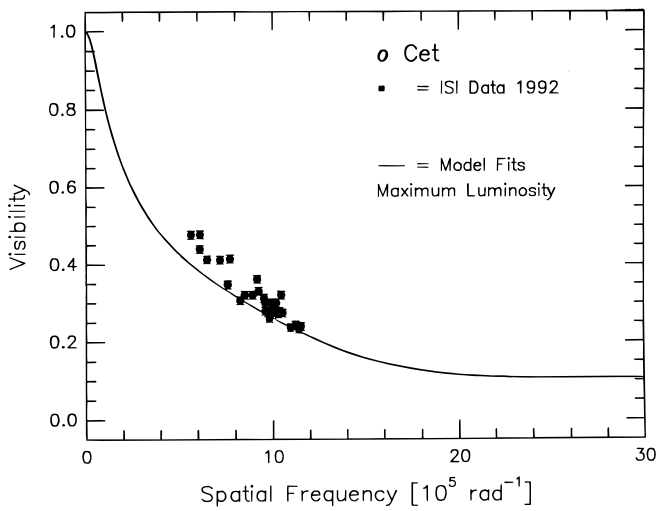


FIG. 7b

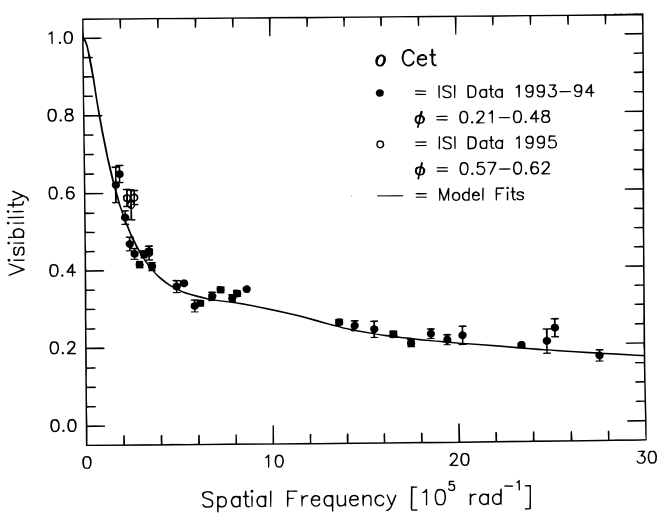


FIG. 7c

FIG. 7.—(*a*) Data for the 1990 (*filled circles*) and 1995 (*open circles*) minimum compared with a dust model (*solid line*) with model parameters from Epoch 1 in Table 4. (*b*) Data (*filled circles*) and model curve (*solid line*) for the 1992 maximum luminosity, with model parameters from Epoch 2 in Table 4. (*c*) Visibility data and model curve for 1993, 1994, and 1995. The 1993 and 1994 data were mostly from $\phi = 0.21$–$0.48$, with model parameters from Epoch 3 in Table 4.

radiative equilibrium relation. This relation equalizes in each torus the total amount of absorbed energy to the total amount of emitted energy provides the temperature of the dust in any torus.

The spectrum of the source as modified by its surrounding dust cloud, the brightness distribution of the source, and corresponding visibility curves as a function of wavelength and inclination of the envelope, are obtained for a given set of parameters characterizing the model. A solution for the parameters is searched empirically until the results of the simulation reproduce the existing measurements.

Since the morphology of the envelope of Mira might not be spherical, three different types of models are examined:

1. Spherical dust shell with an aspherical inner cavity;
2. Disk structure around the star;
3. Clump(s) of dust in the envelope.

The visibilities predicted from these models vary with the hour angle of the interferometer due to baseline rotation. This means that visibility curves calculated from the models will have two branches when they are plotted as a function of spatial frequency (cf. Figs. 3 and 10). However, the difference in visibility between the two branches is small due to the fact that the baselines are primarily east-west in direction. The variation in the observed visibilities is large enough compared to the expected variation in visibility with hour angle from the models that a detailed analysis with hour angle is not warranted at this time.

### 5.1. *Spherical Dust Shell with an Aspherical Inner Cavity*

The assumption of dust fully condensed and distributed uniformly at the inner radius of the dust shell is probably much too simple a description of reality. There are several reasons why the inner cavity could be nonspherical. For example, the mechanism by which gas is lifted from the stellar photosphere and partially condenses into dust grains is not well known. The presence of clumps rather than homogeneous condensation may be expected and it is easy to imagine that the clumps are not necessarily spatially uniform in a spherical inner region. The arrangement of SiO maser emission observed by Greenhill et al. (1995) around the late-type star VX Sgr suggests the presence of dense velocity coherent structures of gas in the extended atmosphere between the photosphere and the inner radius of the dust shell. The characteristic size of the structures is about 0.4 AU. The presence of large hot spots on the stellar photosphere may also affect the shape of the inner region of the dust shell (Tuthill et al. 1995). The radiated light from a hot spot can evaporate some dust of the inner environment in a nonisotropic way and illuminate other regions in a nonuniform way. Variations in the intensity of these hot spots can occur over a timescale comparable with observed variations of the visibility. In addition, measurements at visible wavelengths indicate an ellipsoidal shape.

Thus, there are many observational reasons for considering nonspherical geometries. We begin discussing the details of the models by examining two different models, each with an ellipsoidal inner cavity. In both, the radial density distribution of the dust follows an $r^{-1.5}$ law, which was appropriate to correctly reproduce the far-infrared flux of the broadband spectrum of Mira. The stellar temperature in the model is 2700 K. A unique grain radius of 0.1 $\mu$m is used. The shape of the inner cavity is different for the two models. Model A has an prolate ellipsoidal inner cavity

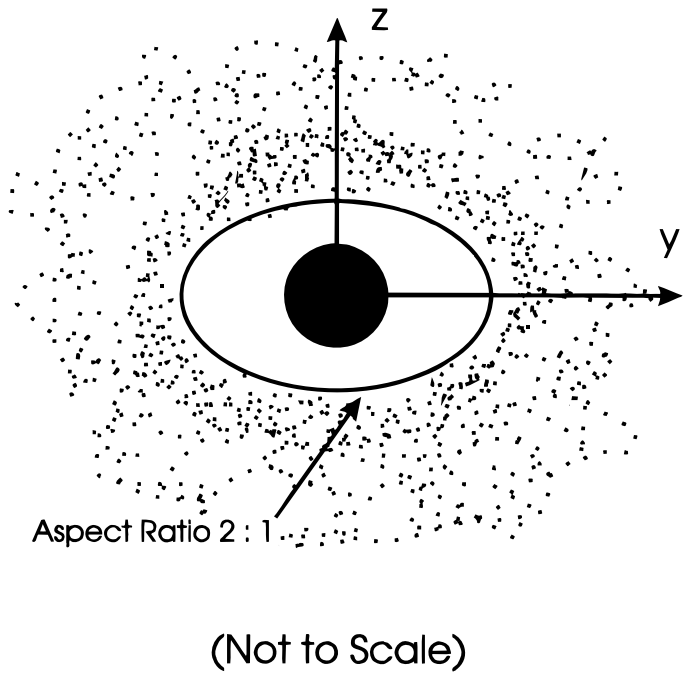


FIG. 8a

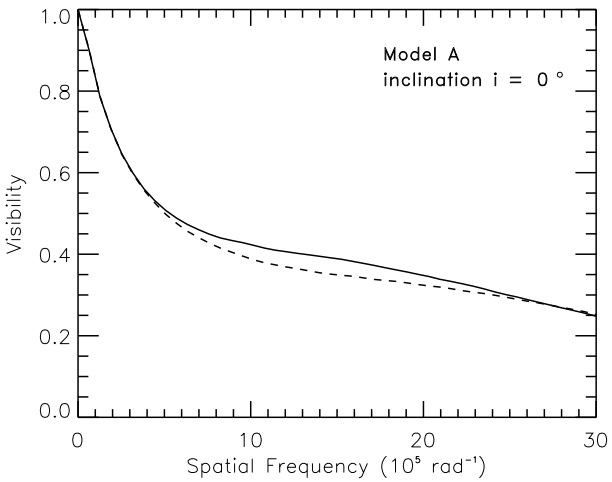


FIG. 8b

FIG. 8.—(*a*) Schematic illustration of the geometry of the ellipsoidal cavity embedded in spherical shell. (*b*) Visibility curves from a model that contains a prolate ellipsoidal cavity with an axial ratio of 2. The solid and dashed curves are for viewing the cavity along the projected minor and major axes, respectively.

with an axial ratio of 2. The dust closest to the star is 2.5 stellar radii from the center of the star, while the further part of the ellipsoid is at 5 stellar radii (see schematic illustration in Fig. 8*a*). The second model (model B) has an oblate ellipsoidal inner cavity with axial ratio of 2 also, and the same characteristics concerning the distances to the extreme parts of the inner region. The optical depth of the two dust shell models varies between 0.1 and 0.14 depending on the direction in which the light passes through the dust shell.

The results of the models are as follows. The optical depth was adjusted to reproduce the broadband spectrum of Mira (Fig. 9). The 11 $\mu$m contour map and the corresponding visibilities, drawn for two opposite directions, are shown on Figure 8*b* for model A. It is interesting to note that the visibilities do not change much from one direction to the perpendicular one. The same remark applies for model B, indicating in both cases that the nonsphericity of the inner cavity (at least for the chosen model parameters) and its possible temporal shape evolution do not explain the larger changes observed between the 1992 visibility measurement and the rest of the data. At 11 $\mu$m, a nonspherical cavity embedded in a spherical shell does not produce a strong effect on the visibility curves, mainly because much of the envelope is hot enough to emit strongly at 11 $\mu$m. Thus, the contribution of the inner region, although perceptible, is not dominant in the formation of the visibility.

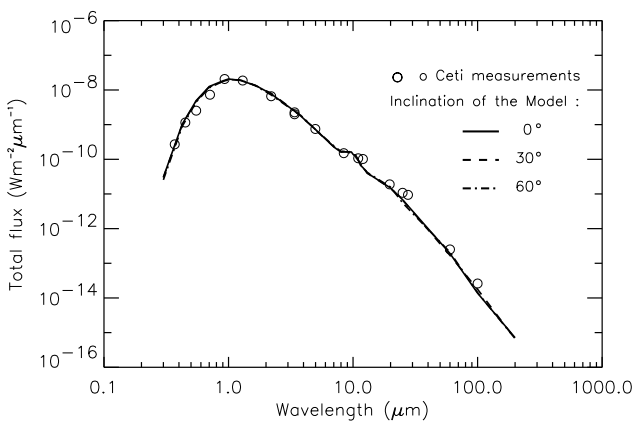


FIG. 9.—Broadband spectrum of o Ceti (*circles*) and model curve for maximum luminosity based on the photometry data referenced in Rowan-Robinson & Harris (1983).

### 5.2. *Disk-shaped Dust Distribution*

Mira stars, from an evolutionary point of view, are in an early stage of the Asymptotic Giant Branch of the Hertzprung-Russell diagram. Optical bipolar nebulae of more evolved type objects like CRL 618 and CRL 2688 (Egg Nebula), which are believed to be post-AGB objects and are in fast transition toward the planetary nebula stage, show clear evidence for a disk structure forming the circumstellar environment. Most post-AGB sources are known to have axisymmetric shapes (Bujarrabal, Alcolea, & Planesas 1992; Meixner 1993). Until now, no surrounding disk of an AGB star has been clearly detected. However, the presence of a bipolar outflow located within the envelope of Mira has been established by Planesas et al. (1990). Two lobes of gas observed in the CO emission line ($J = 2$–1) support the idea of asymmetries in the envelope of Mira and are interpreted as the result of the partial collimation of the wind by a higher density region in the equatorial plane of the object.

The structures at large spatial scales in the dust shell (larger than both clumpiness and the dimensions of the inner cavity) may significantly affect the 11 $\mu$m visibility curves. Some disk structure models for Mira were processed. The density law employed is the product of a func-

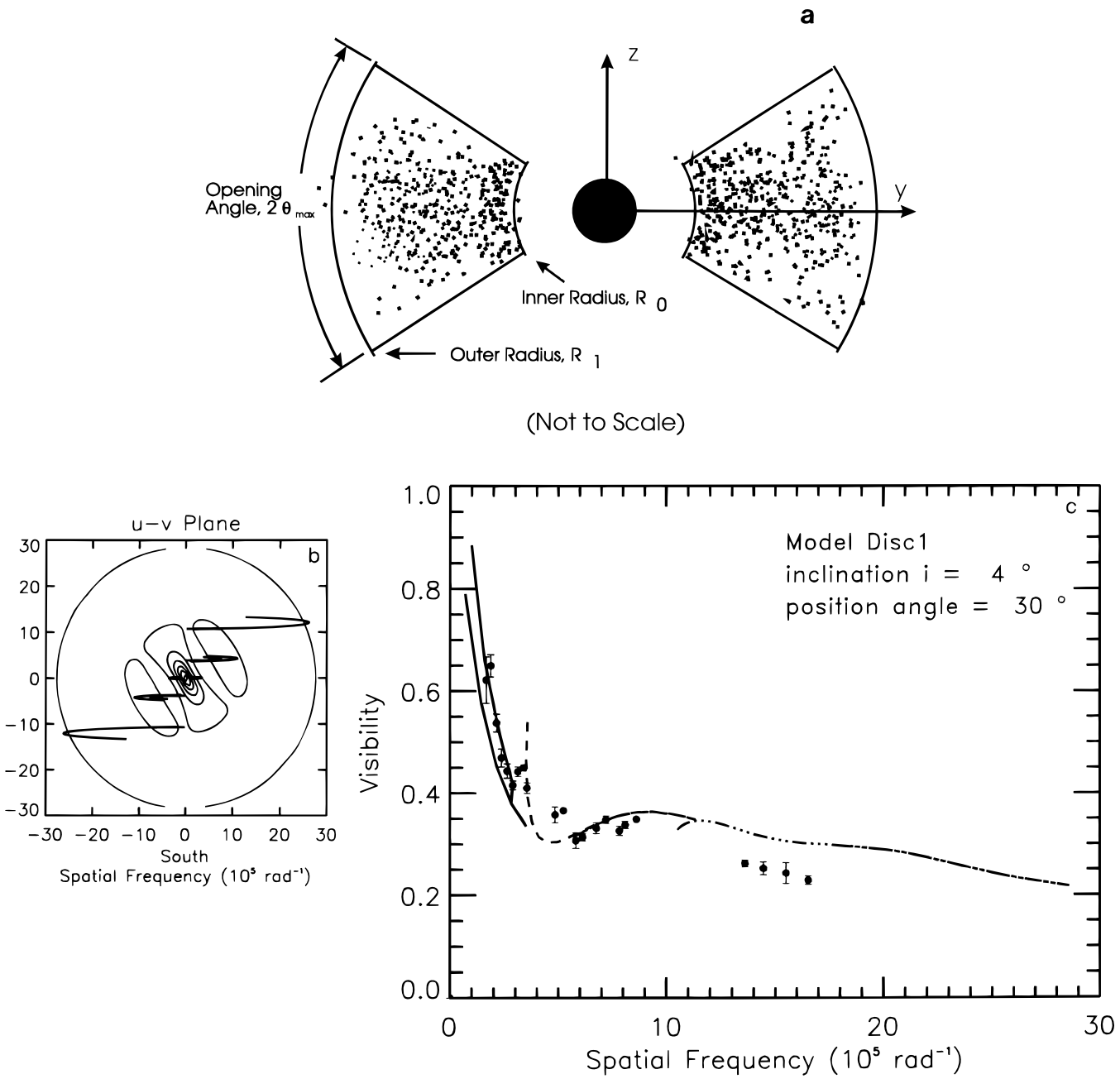


FIG. 10.—(*a*) Schematic illustration of a slice cut through the center of the disk model. The inner radius of the dust, the opening angle of the disk, the inclination of the disk with respect to the line of sight, and the position angle of the axis of revolution are all parameters of the model; (*b*) Contours of the two-dimensional model visibility amplitudes superimposed on the ($u$, $v$) tracks of the ISI data; (*c*) Visibility data (1993–1994) (*filled circles*) and visibility curve from the model Disk1, with disk inclination 4° and position angle 30°. The visibility curves are drawn with three different line types corresponding to the ($u$, $v$) tracks from which they are calculated from the left panel. The solid line represents ($u$, $v$) track from the 4 m baseline, the dashed line represents the 9 m baseline, and the dash-dotted line represents the 32 m baseline.

tion of $r$ and $\theta$, $n(r, \theta) = f(r)g(\theta)$, where $\theta$ is the latitude angle from the plane of the disk. The results of the following two models are obtained for a radial density law $f(r) = r^{-1.5}$. The function $g(\theta)$ is a decreasing function from $\theta = 0$, i.e., the equatorial plane, up to $\pm 40°$, thus $[g(\theta) = 1 + \cos(\theta \times 180°/40°)]$. The function $g(\theta) = 0$ when the absolute value of $\theta$ is greater than 40°. The stellar temperature in both models is equal to 2800 K, and a unique grain size was used, $a = 0.1$ $\mu$m. Both models remain consistent with the broadband spectrum of Mira. The angular radius of the star is set to 19 mas to provide the measured flux level.

The first disk model, Disk1, assumes the dust is present from an inner radius of 10 $R_*$ to 800 $R_*$, where $R_*$ denotes the stellar radius, as shown schematically in Figure 10*a*. The optical depth at 11 $\mu$m in the equatorial plane is 0.09. The model visibility map with the ($u$, $v$) tracks from the ISI baseline in the Fourier plane are displayed in Figures 10*b* and 10*c* together with the set of measured visibility curves and the visibility extracted from the model. The best orientation for the disk in terms of fitting the 1993–1994 visibility data for an inclination angle of 4°.5 of the disk with respect to the line of sight as seen in Figures 10*b* and 10*c*. The position angle of the axis of revolution of this model, mea-

sured from north to east, is about 30°. The global shape of the 1993–1994 observed visibility with its bump located at approximately 7–8 $\times$ $10^6$ rad$^{-1}$ is reproduced with such a disklike structure.

Model Disk2 is slightly different. The inner edge of the disk of dust is now closer to the star, $R_0 = 3\ R_*$. The optical depth in the plane of the disk at 11 $\mu$m is 0.12. This alternative model results in a better overall fit to the 1993–1994 visibility data. However, the bump feature has now disappeared as a result of the inner edge of the dust shell being closer to the star than in the previous model. Figures 11*a* and 10*b* display the visibility data and model visibility curve

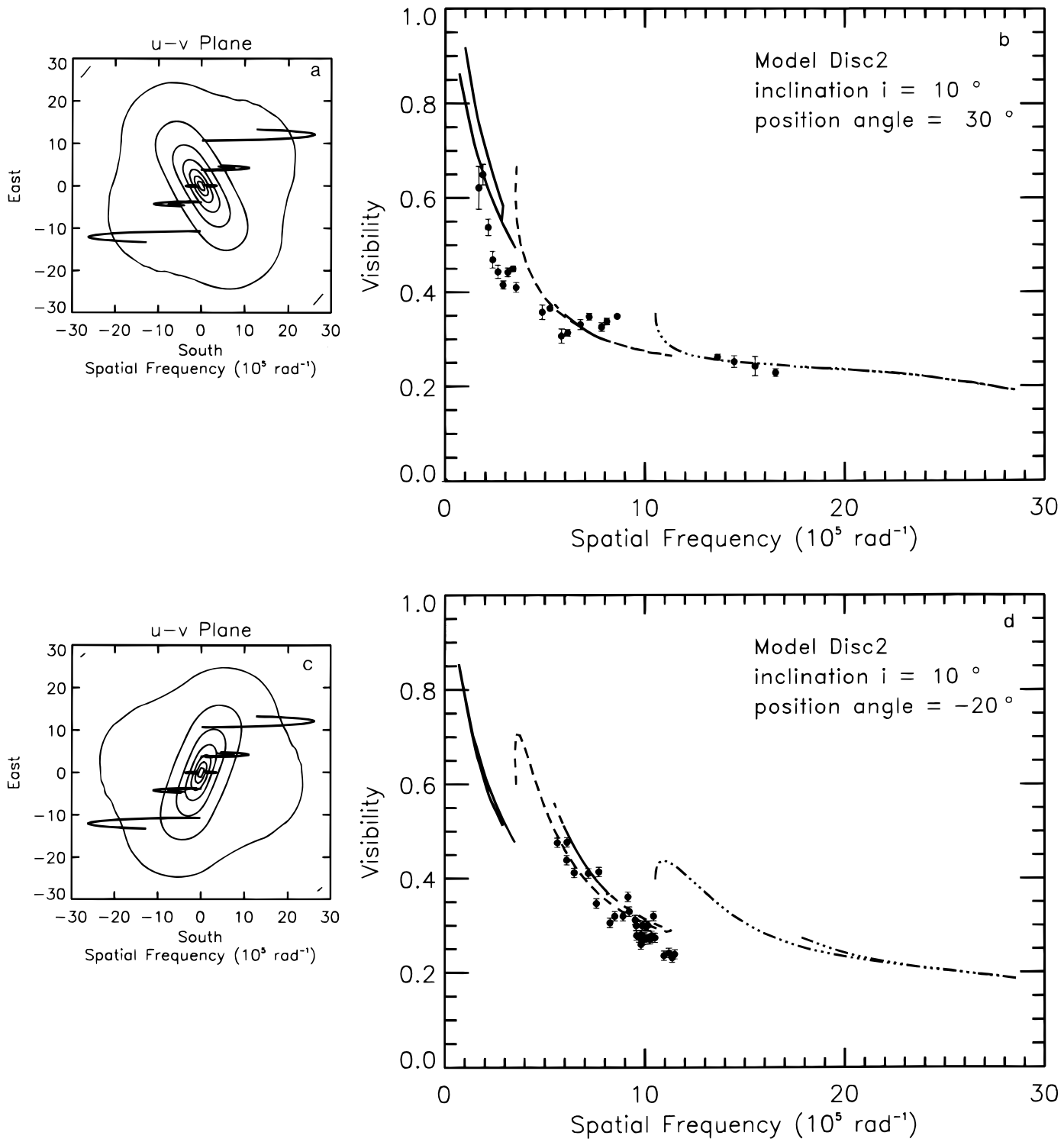


FIG. 11.—(*a*) Contours of the two-dimensional model visibility amplitudes superimposed on the (*u*, *v*) tracks of the ISI data for model Disk2 with inclination 10° and position angle 30°; (*b*) Visibility data (1993–1994) (*filled circles*) and visibility curve from the model Disk2 for the model parameters of panel (*a*); (*c*) Contours of the two-dimensional model visibility amplitudes superimposed on the (*u*, *v*) tracks of the ISI data for model Disk2 with inclination 10° and position angle −20°; (*d*) Visibility data (1992) (*filled circles*) and visibility curve from the model Disk2 for the model parameters of panel (*c*).

for a disk inclination of 10° and a position angle of 30°. Figures 11*c* and 11*d* show that the shape of the 1992 visibility data is now correctly fitted by the model with the position of the object rotated with respect to the plane of the sky (position angle −20°).

The power spectra of Mira observed by Karovska et al. (1991) at three different wavelengths are reproduced in Figure 12. Their data were taken from 1987 December 30 to 1988 January 3, corresponding to a stellar phase, $\phi = 0.97$. The shapes obtained for the simulated power spectra agree well with the data. The elongations of the model spectra increases when the wavelength is shortened. This behavior is thus consistent with the observations, but the orientation of the large axis of the Karovska power spectra (about 115°

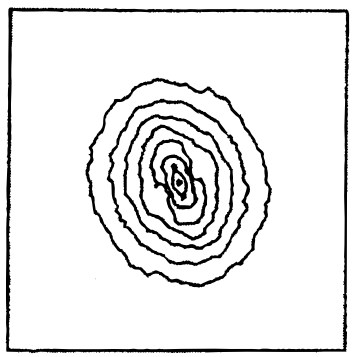

FIG. 1*a*

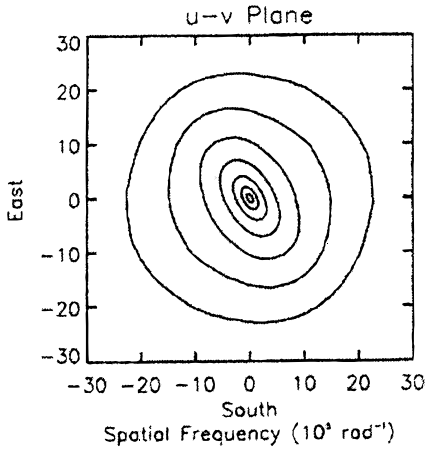


FIG. 1*b*

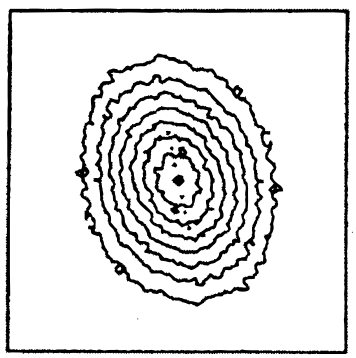

FIG. 1*c*

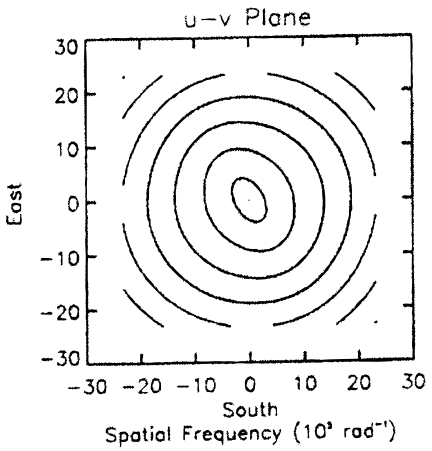


FIG. 1*d*

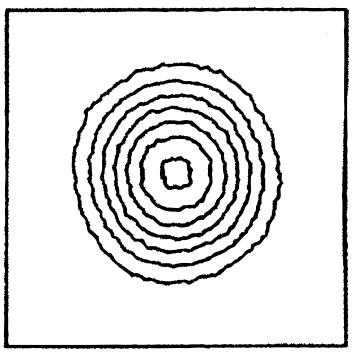

FIG. 1*e*

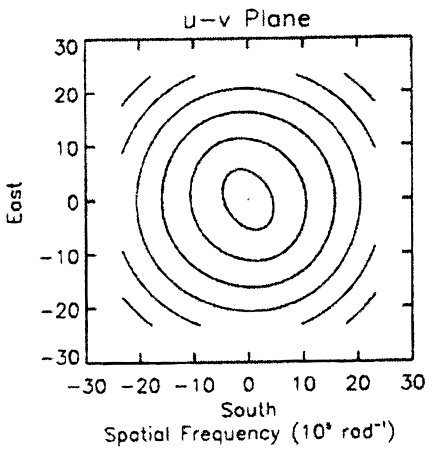


FIG. 1*f*

FIG. 12.—(*a*, *b*) Upper two panels display contours of the two-dimensional visibility amplitude distributions from the speckle data of Karovska et al. (1993) at a wavelength of 0.55 μm and the model Disk2, at 0.533 μm, respectively; (*c*, *d*) Middle two panels display two-dimensional visibility amplitude distributions from the speckle data of Karovska et al. (1993) at 0.775 μm and the model Disk2 at 0.78 μm, respectively; (*e*, *f*) Bottom two panels display two-dimensional visibility amplitude distributions from the speckle data of Karovska et al. (1993) at 0.855 μm and the model Disk2 at 0.85 μm, respectively.

from north) is not explained with the geometrical orientation presented in Figures 11*a* and 11*b*.

Asymmetries at large scale in the dust shell, such as a disk structure, thus present some attractive properties in agreement with part of the data. The characteristics of the 1993–1994 visibility curve are well reproduced. Also, even if the orientation of the elongation of the observed visible power spectra of Mira appears to be different from the best orientation, allowing a good 11 $\mu$m visibility fit, the shapes of the visible power spectra observed/modeled agree reasonably well. This shows that scattering from large-scale asymmetric structures in the shell may cause the object image to deviate from circular symmetry.

However, one must conclude that, as attractive as the disk structure may be to explain part of the data, the rotation in position angle from 30° to −20°, which, as suggested by the model Disk2, reproduces the cycle-to-cycle variation of the visibility curves, is obviously nonrealistic. A year timescale is obviously much too short a time for the motion of such large structures. Other possible events in the environment of the star are more consistent with the observed temporal variations, as we discuss below.

### 5.3. *Clumps in the Circumstellar Shell of Mira May Explain the Unusual 1992 Visibility Curve*

Clumps of dust are probably present in the environment of Mira. As mentioned in a previous section, clumpiness rather than homogeneous condensation close to the star, for example, is supported by the SiO maser observations of VX Sgr (Greenhill et al. 1995). In this section three different hypotheses concerning the disposition of the clump(s) in the circumstellar environment of Mira are presented.

Although large-scale structures of the envelope may exist, a common element of the next set of models tested is that the clumps are embedded in a spherically symmetric dust shell of lower density. The inner radius of the dust shell varies between 2.6 and 5 $R_*$, depending on the model. The first sequence of models is named Clump1; the parameters are displayed in Figure 13. The model Clump1(a) contains one big clump of dust of radius 8 $R_*$ and located at a distance of 28 $R_*$ from the center of the star. The density of dust in the clump is about 120 times the density in the close surrounding region. The optical depth of the shell through the clump is 0.86 at 11 $\mu$m. Distinct sizes of clumps were used for the simulation with radii between 5 and 8 $R_*$, no sensitive differences were found on the visibility. The inner radius of the spherical part of the model is 5 $R_*$. A stellar temperature of 2600 K is assumed. The angular stellar radius is 21 mas. Figure 14 shows the visibility curve of this model with the Fourier map, which contains the $(u, v)$ tracks of the interferometer sampling. The visibility shows several wiggles attributed to the dual structure of the model (star + clump). The first wiggle occurs at approximately $4 \times 10^5$ rad$^{-1}$. The visibility data presents a gap in this region and whether the existence of the wiggle is real or not is not established. The best geometrical position of the clump with respect to the star, which allows a reasonable fit to the visibility measurements, is the following: the axis containing the star and the clump is tilted by an angle of 15°.5 with the plane of the sky. The position angle of this axis projected onto the plane of the sky is 120° modulo 180°. This model is consistent both with the shape of the broadband flux and with the 11 $\mu$m flux level of Mira.

At low spatial frequencies the position of this first wiggle in the visibility is linked to the relatively distant location of the clump of dust from the star. The location of the clump is interesting because the dust temperature in this region, according to the model parameters used, ranges between 311 and 352 K. Considering these temperature values, the 11 $\mu$m wavelength of observation is in the edge of the expo-

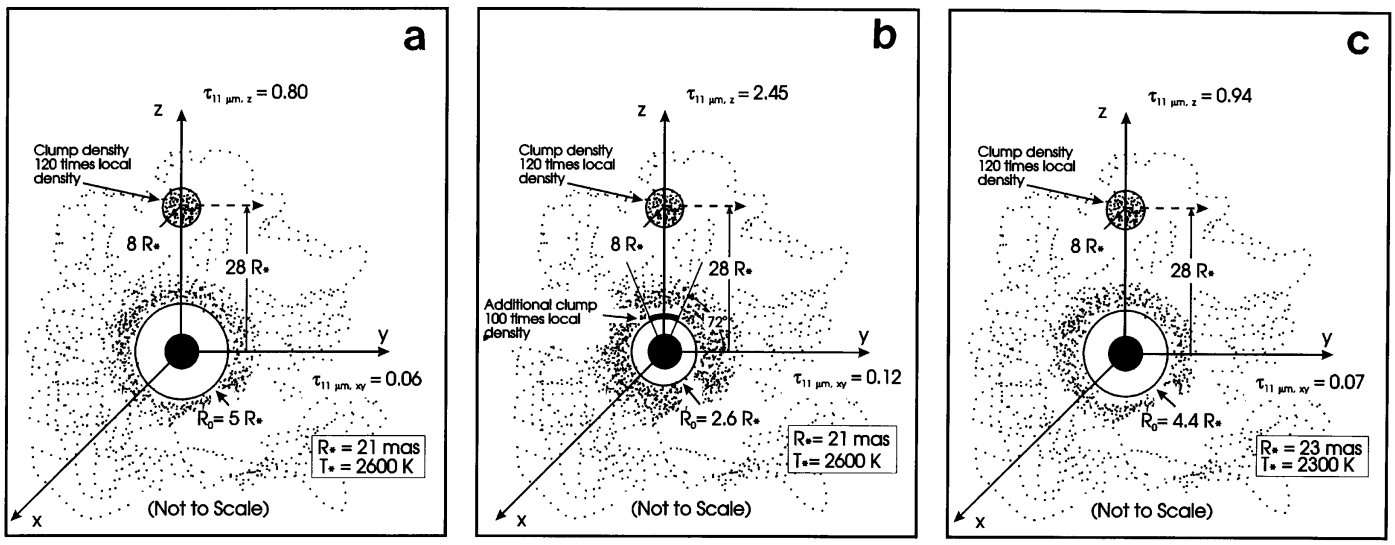


FIG. 13.—(*a*) Schematic illustration of model Clump1(a), which consists of a spherical dust shell with a $r^{-2}$ density distribution beginning at 5 $R_*$ and an additional clump of dust 120 times as dense as the local density of dust. This clump is spherical in shape, with a radius of 8 $R_*$, located at a distance of 28 $R_*$ along the $z$-axis from the star. This model corresponds to the 1993–1994 visibility measurements. (*b*) Schematic illustration of model Clump1(b), which is based on the model Clump1(a), but with the following changes, first, the inner radius of the dust has shrunk from 5 to 2.6 $R_*$, and second, an additional clump of dust has appeared along the $z$-axis just outside the inner edge of the dust shell. This clump looks like a spherical shaped cap, and subtends a half-angle of 22° viewed from the center of the star. The density of this dust is 100 times the surrounding density; the total optical depth of dust along the $z$-axis has increased from 0.8 to 2.45 at 11 $\mu$m, and the optical depth of dust along the $x$-$y$ plane has increased from 0.06 to 0.115. This model corresponds to the 1992 epoch. (*c*) Schematic illustration of model Clump1(c), which is similar to model Clump1(a), assumes that the clump of dust close to the star in model Clump1(b) has evaporated, as has much of the dust in the spherical shell, close to the star. This leaves the star with a dust shell beginning at 4.4 $R_*$, and the optical depth along the $z$-axis is 0.94, while the optical depth along the $x$-$y$ plane is 0.07. This model corresponds to the 1990 epoch.

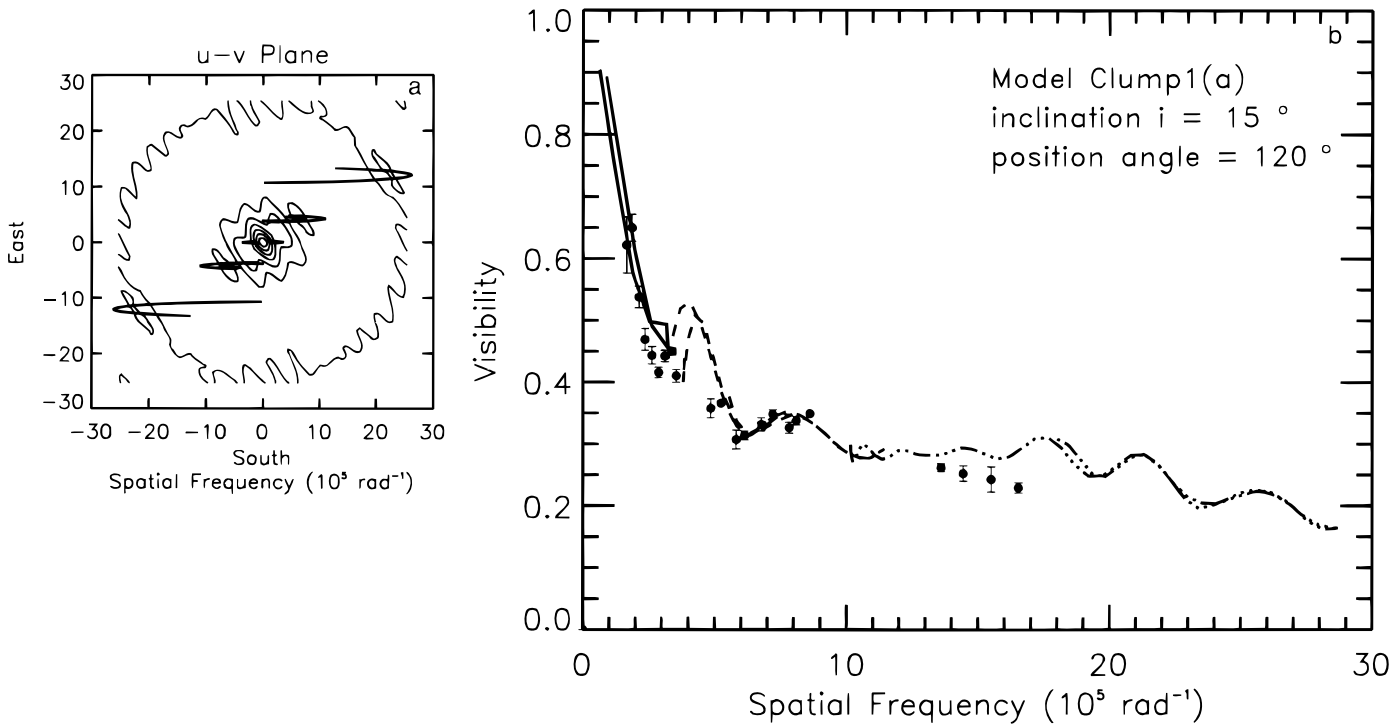


FIG. 14.—(*a*) Contours of the two-dimensional model visibility amplitudes superimposed on the *u-v* tracks of the ISI data for model Clump1(a) with inclination 15° and position angle 120°; (*b*) Visibility data (1993–1994) (*filled circles*) and visibility curve from the model for the model parameters of Figs. 13*a* and 14*a*.

nential regime of the Planck function for the grain emission. This means a dark spot on the stellar photosphere in the same direction as the clump of dust, or an additional intermediate clump of dust shading the stellar radiation toward the furthest clump, can strongly decrease its contribution to the 11 $\mu$m visibility curve. Being in the exponential regime of the Planck function magnifies the effect. The scenario of the additional clump has been successfully tested in model Clump1(b). The additional clump of dust is very close to the star, between 2.6 and 3 $R_*$, from the center of the star, and is 100 times denser than the local surrounding environment. The optical depth of the new clump is 1.6 at 11 $\mu$m. Another change from the first model, Clump1(a), concerns the dust of the spherical dusty part of the envelope, which in Clump1(b) is as close as at 2.6 $R_*$ from the center of the star. The star has the same characteristics (temperature and angular size) as in model Clump1(a). Figure 15 presents the processed visibility and the successful fit of the 1992 measurements.

The model Clump1(c) is also derived from model Clump1(a). The effective stellar temperature is now 2300 K (minimum phase of luminosity of Mira). The effective angular radius increases to 23 mas. The geometry and optical depth of the dust shell do not change much from model Clump1(a), the original inner radius was only reduced by 5% in size. Figure 16 compares the 1990 visibility measurements taken during minimum phase to this model. A reasonably good fit is obtained.

Hence, such a set of models shows that the scenario of formation/destruction of a clump of dust shading the stellar light may under certain conditions produce the variations observed in the visibility data. Moreover, an evolution mainly of the stellar temperature and size of the model may also explain the 1990 visibility measurements taken during a minimum phase of luminosity.

Model Clump2 is nearly identical to model Clump1. It is a symmetrization of the clump in model Clump 1 with regard to the star. In addition to the clump of dust of model Clump1(a), the presence of an identical and symmetric clump also produces model visibilities that fit the 1993–1994 visibility data. The 11 $\mu$m optical depth along the *z*-axis is in this case 0.52, a value 60% lower compared to model Clump1(a). In a similar way to the changes applied from model Clump1(a) to Clump1(b), the decrease of the size of the inner shell cavity (from 5.5 to 2.6 $R_*$) associated with the presence near the star and now at each side of the star of intermediate clumps that shade the stellar radiation propagating toward the further clumps, generate some variations on the visibility compatible to those observed in 1992. The optical depth of the intermediate clumps must be around 1.6–1.8 at 11 $\mu$m.

A drop of the effective temperature from 2600 to 2300 K in the symmetrized model of model Clump1(a) explains the measured visibility curve of 1990 taken during minimum luminosity of Mira.

In the present stage the ISI is an interferometer comprised of two telescopes. This makes it practical to determine only the modulus of the Fourier transform of the object. Hence, it is not possible to discriminate which model (Clump1 or Clump2) is the more realistic one. The plausible asymmetries caused by clump(s) of dust at only one side of the star could be confirmed by a measure of the phase of the object Fourier transform, which should vary in this case.

Clump3 is another set of hypothetical models. In this model several partial thin shells of dust comprise the dust geometry (see Fig. 17). These multishells or clumps may be the result of the periodic formation of dust. This situation has a practical interest: if the partial shells of dust are

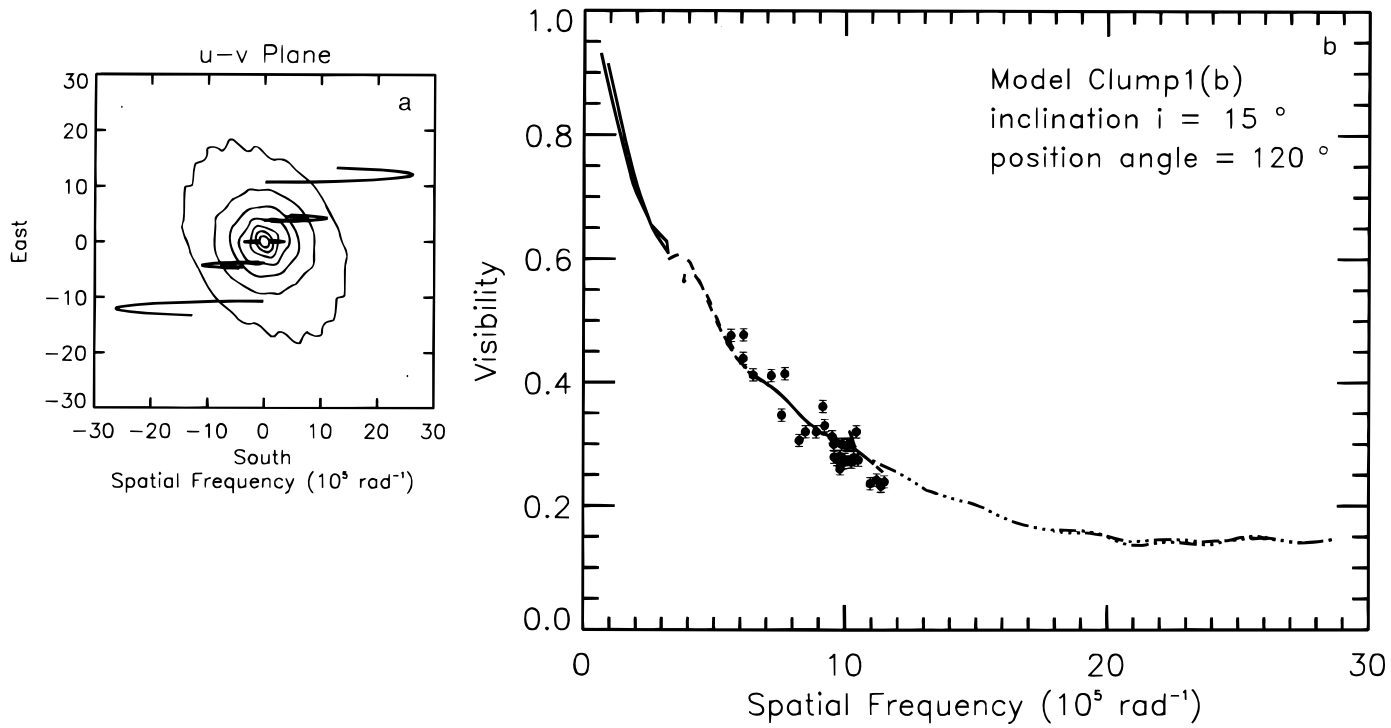


FIG. 15.—(*a*) Contours of the two-dimensional model visibility amplitudes superimposed on the *u-v* tracks of the ISI data for model Clump1(b) with inclination 15° and position angle 120°; (*b*) Visibility data (1992) (*filled circles*) and visibility curve from the model for the model parameters of Figs. 13*b* and 15*a*.

aligned and equidistant, they contribute to the visibility curve by accumulating some energy in a given spatial frequency range. In other words, a periodic structure in the object may explain the bump observed in the 1993–1994 visibility. A new partial shell of dust forming may lead to the changes observed in the 1992 measurements.

Model Clump3(a) contains four partial shells of dust, whose geometry is detailed in Figure 17. The partial shells each have density 30 times that of the local dust density. The optical depth of the envelope at 11 $\mu$m through the

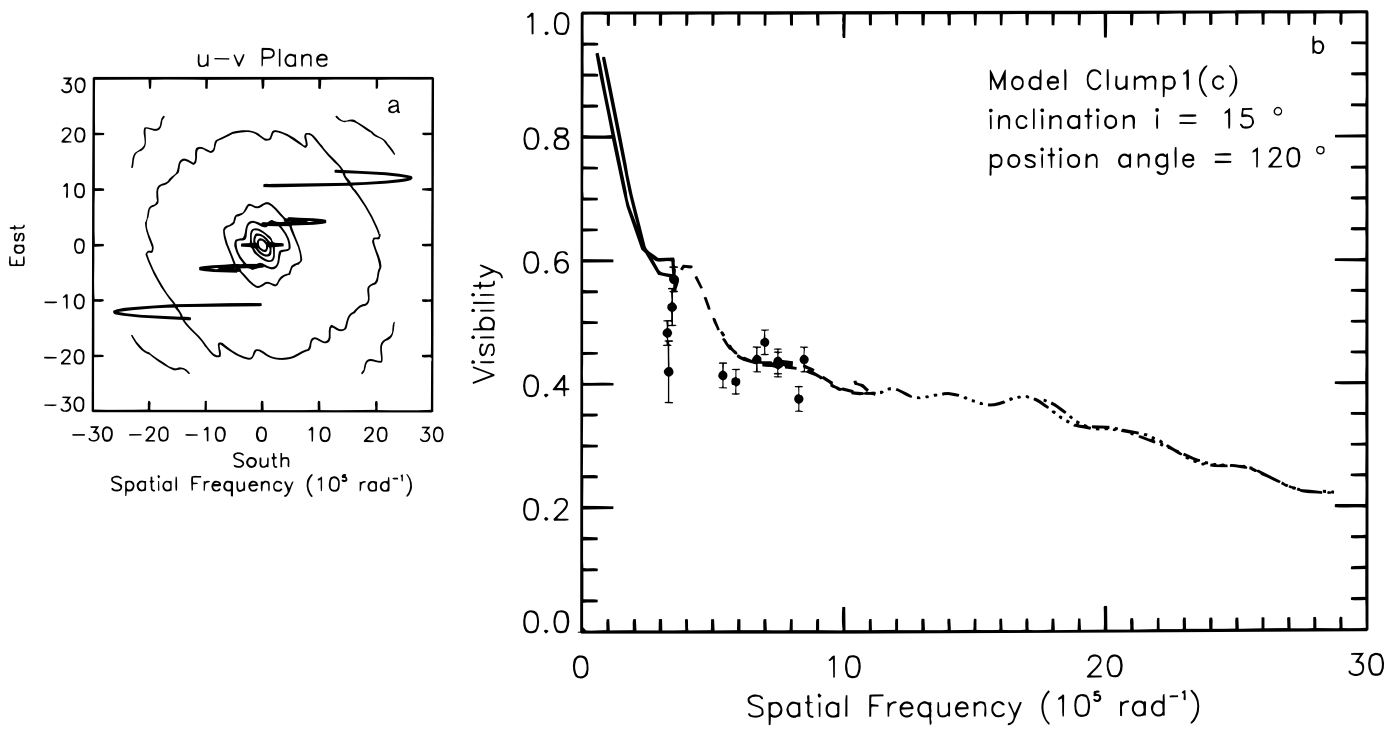


FIG. 16.—(*a*) Contours of the two-dimensional model visibility amplitudes superimposed on the *u-v* tracks of the ISI data for model Clump1(c) with inclination 15° and position angle 120°; (*b*) Visibility data (1990) (*filled circles*) and visibility curve from the model for the model parameters of Figs. 13*c* and 16*a*.

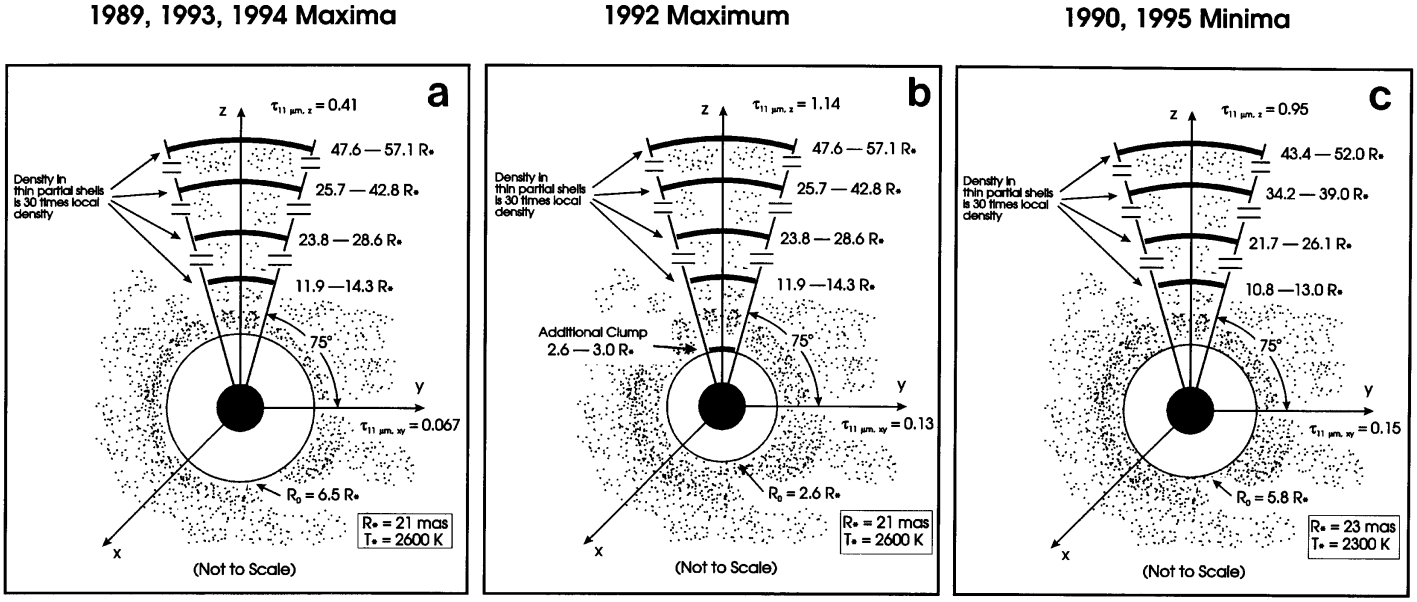


FIG. 17.—(*a*) Schematic of model Clump3(a), which consists of a set of spherically shaped thin dust caps, with opening half-angles of 25° as viewed from the star. The dust caps are from 11.9–14.3 $R_*$, 23.8–28.6 $R_*$, 35.7–42.8 $R_*$, and 47.6–57.1 $R_*$, respectively. The inner radius of the dust shell is at 6.5 $R_*$, while the optical depth along the *x*-*y* plane is 0.067 and is 0.41 along the *z*-axis. These clumps are embedded in a spherical dust shell and have a density 10–30 times greater than the surrounding dust. (*b*) Model Clump3(b) is the same as model Clump3(a), but with the inner radius of the dust now at 2.6 $R_*$, and with an additional clump of the same shape as before, from 2.6–3.0 $R_*$. The optical depth along the *x*-*y* plane becomes 0.13, while that along *z*-axis becomes 1.14. (*c*) Model Clump3(c) is the same as model Clump3(b) but with the inner radius slightly smaller than that of Clump3(a), 5.8 $R_*$, and the 11 $\mu$m optical depth is 0.95 along the *z*-axis and is 0.15 along the *x*-*y* plane.

partial dust shells is 0.41. The star has a temperature of 2600 K and an angular diameter of 21 mas. The visibility curve obtained from this model is shown in Figure 18. The evolution of the visibility toward the one observed in 1992 can be as previously (models Clump1 and Clump2) produced by the presence of an additional partial shell of dust. The extra clump located at about 3 $R_*$ from the center of the star has an 11 $\mu$m optical depth of 0.73. The synthetic visibility from model Clump3(b) is presented in Figure 19. While the 1992 data are reasonably well reproduced, the fit of the data is

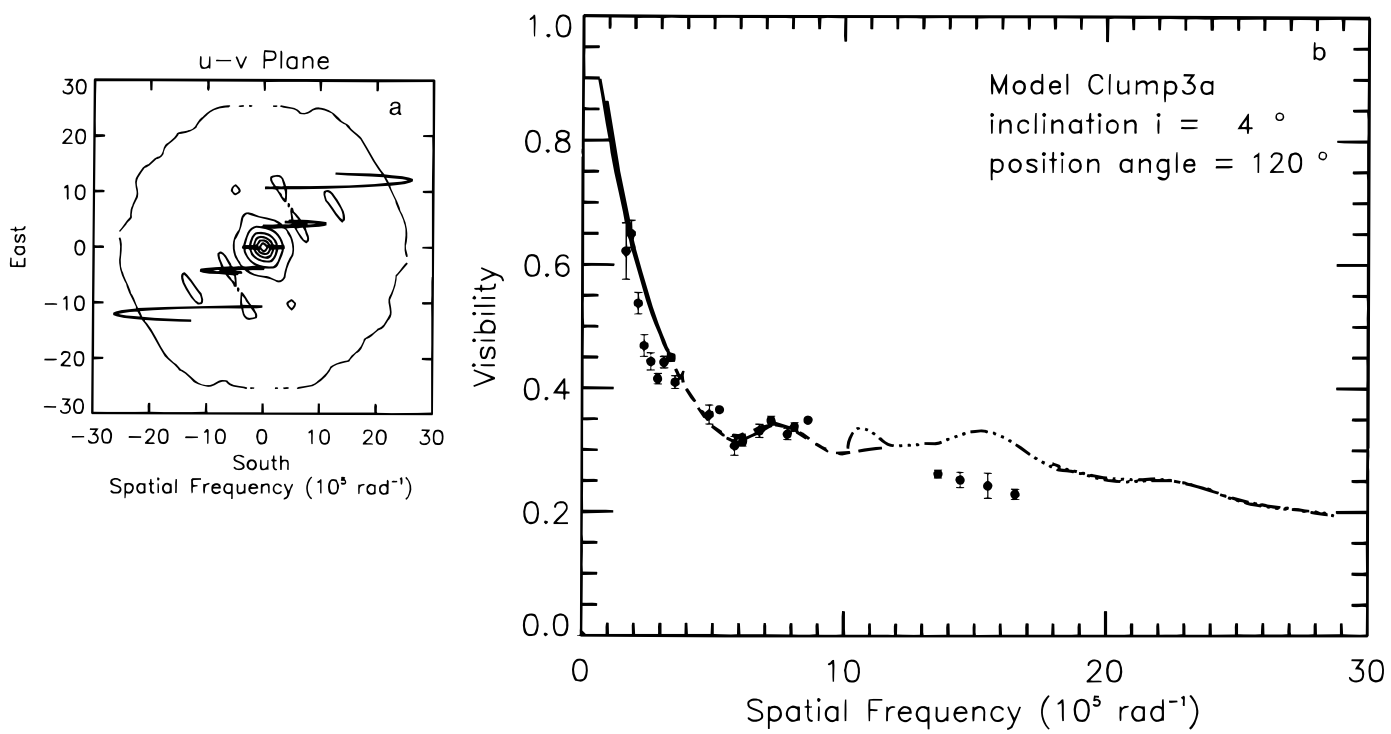


FIG. 18.—(*a*) Contours of the two-dimensional model visibility amplitudes superimposed on the *u*-*v* tracks of the ISI data for model Clump3(a) with inclination 4° and position angle 120°; (*b*) Visibility data (1993–1994) (*filled circles*) and visibility curve from the model for the model parameters of Figs. 17*a* and 18*a*.

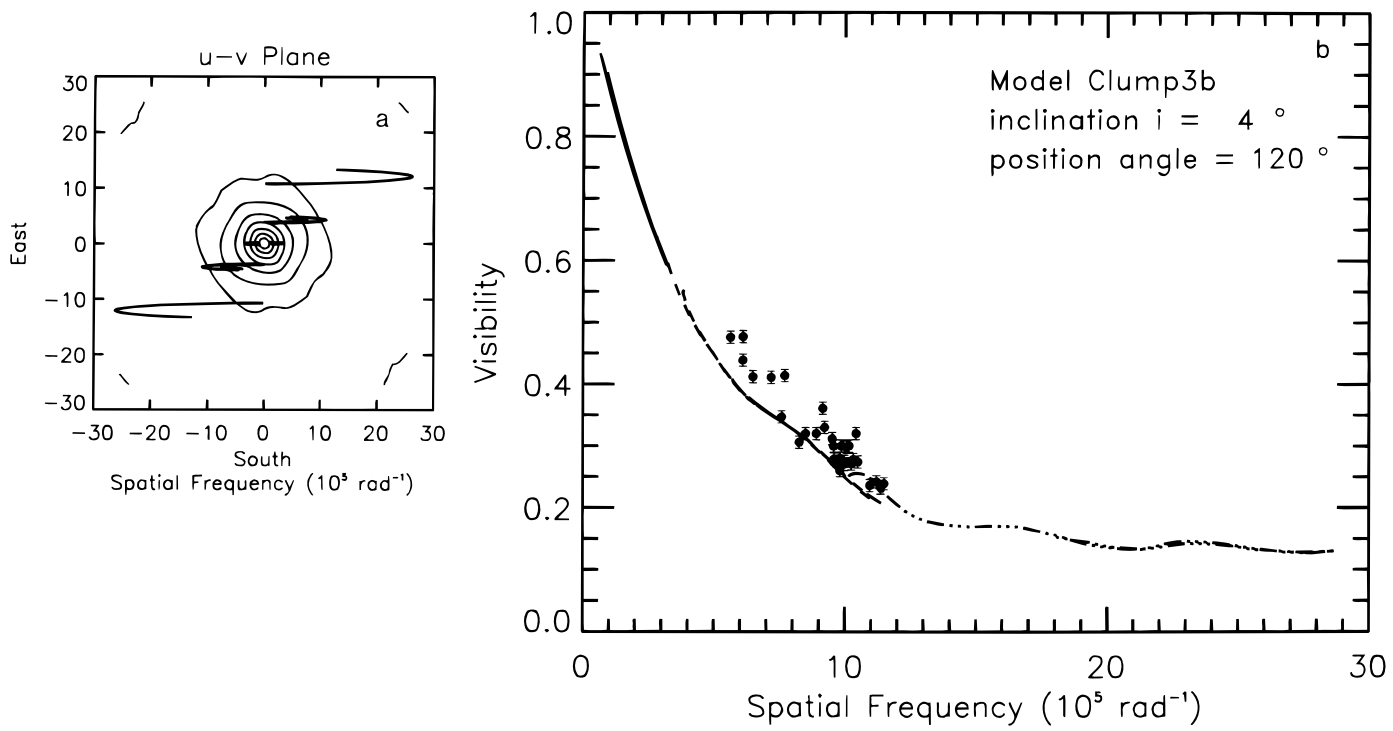


FIG. 19.—(*a*) Contours of the two-dimensional model visibility amplitudes superimposed on the *u-v* tracks of the ISI data for model Clump3(b) with inclination 4° and position angle 120°; (*b*) Visibility data (1992) (*filled circles*) and visibility curve from the model for the model parameters of Figs. 17*b* and 19*a*.

not as perfect as the one obtained from model Clump1(a). We think it is not possible at the present stage to say that one set of models (Clump1/Clump3) is better than the other at explaining the data. The set of models, Clump3, represents another plausible hypothesis. The 1990 visibility observed during minimum of Mira and fitted by model Clump3(c), is shown in Figure 20. The angular dimensions and characteristics of the envelope are roughly the same as

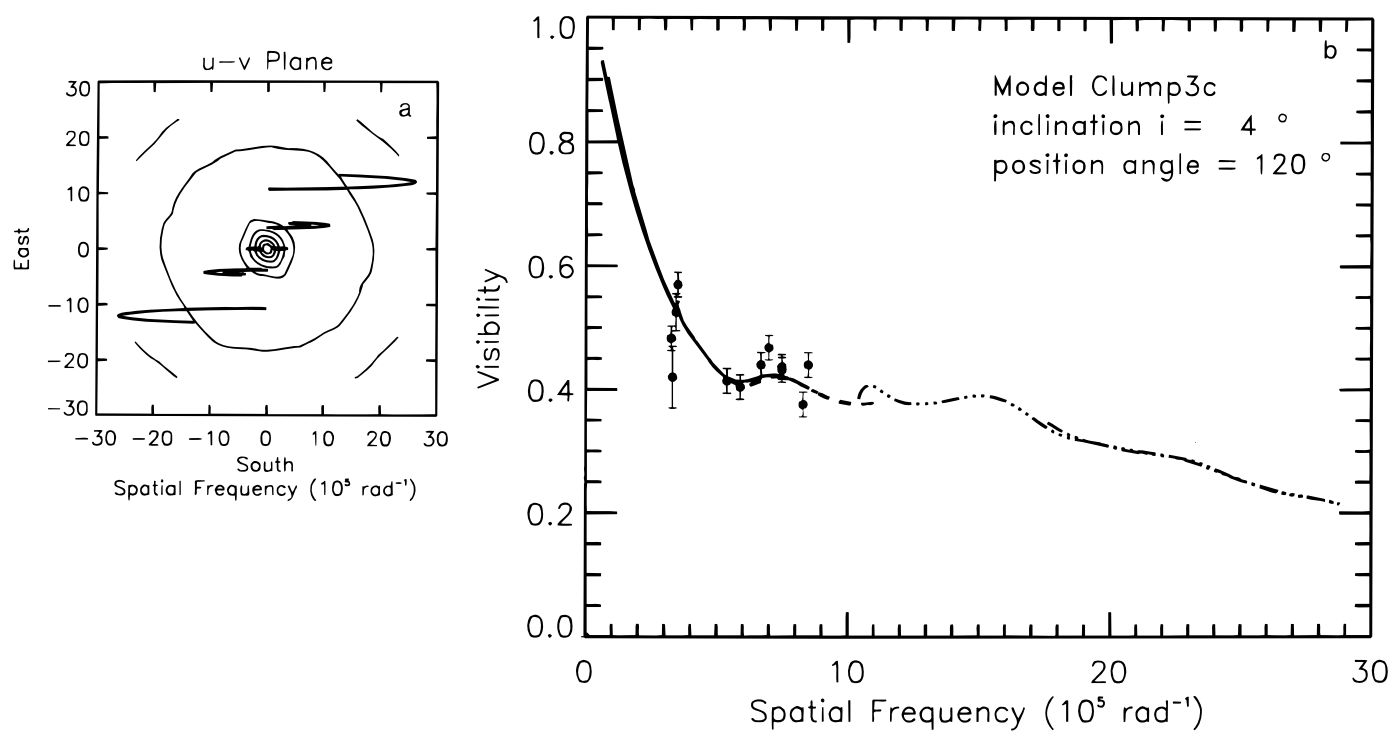


FIG. 20.—(*a*) Contours of the two-dimensional model visibility amplitudes superimposed on the *u-v* tracks of the ISI data for model Clump3(c) with inclination 4° and position angle 120°; (*b*) Visibility data (1990) (*filled circles*) and visibility curve from the model for the model parameters of Figs. 17*c* and 20*a*.

model Clump3(a). The effective temperature is lowered to 2300 K. The angular diameter of the star is set to 23 mas.

## 6. DISCUSSION

Both spherical and nonspherical models of the dust shell of Mira provide scenarios that can explain the evolution of the 11 $\mu$m visibility data. But each requires substantial variations in dust density with distance from the star and with time. Additional degrees of freedom are added to the modeling of the Mira and its envelope when aspherical structures are presumed to exist in the circumstellar environment as compared to the simpler spherical models. Several sequences of models make sense in terms of their ability to fit the observed visibilities; nevertheless each of the scenarios is still hypothetical. There is as yet no criteria to determine a realistic and unique solution. A discussion of the sequences of models with some other relevant results obtained for o Ceti is given below.

Position measurements of the known companion of Mira made by Karovska et al. (1993) give a separation of 0".61 and position angle of 112°. The orbital period of the companion being at least 400 years (P. Couteau 1994, private communication), its position can be considered approximately fixed with regard to the set of ISI measurements, which were made over a time period of only a few years. The set of models Clump1 is characterized by a large (8 $R_*$) and far away clump of dust (28 $R_*$ of distance from the center of the star). The separation of the clump from the star is about 0".55 and the position angle of the clump is about 120° with an ambiguity of 180°. It is interesting to note that a physical link may possibly exist between the best position of the large clump (determined from the modeling) and the position of the companion.

Evidence for an accretion disk formed around the companion of Mira is discussed in the paper of Reimers & Cassatella (1985). Ultraviolet spectroscopic observations made by the *International Ultraviolet Explorer* (*IUE*) imply the existence around Mira B of a thin, rotating disk with a radius of about $10^{11}$ cm. The mass of the disk is estimated to be $5 \times 10^{-13}$ $M_\odot$. The 8 $R_*$ radius clump of dust in model Clump1 is about 2000 times larger than the size of the assumed accretion disk and its mass is of the order of $3 \times 10^{-9}$ $M_\odot$. Furthermore the electron temperature of the accretion disk observed by Reimers and Cassatella is about 11,000 K. Hence, the part of the o Ceti envelope where the 11 $\mu$m continuum emission originates must be distinct from this. Modulation in the UV brightness discussed by Reimers & Cassatella (1985) could be due to variability of the mass accretion rate of the companion caused by the variable mass-loss rate of Mira A implied by the models discussed in this paper.

All plausible sequences obtained from spherical and asymmetrical models of the dust shell indicate that a newly condensed clump of dust near the star may explain the changes contained in the peculiar 1992 visibility curve. This hypothetical clump has to be formed in 1992 and destroyed just after 1992 in order to recover the shape of the visibility curve observed in 1993–1994. An unusually bright visible magnitude during this period gives some credence to this possibility.

Dynamical models of dust formation around late-type stars, reported in the paper of Winters et al. (1995), include time-dependent hydrodynamics and a detailed treatment of the processes of dust formation, growth, and evaporation. Although the stellar environment is assumed to be carbon rich in these models, the results obtained can be qualitatively compared to our Clump3 sequence of models. Indeed, Winters et al. (1995) showed that dust can be formed in discrete layers around the star producing a visibility curve with temporal changes comparable to what is observed in the 11 $\mu$m visibilities. In addition, Fleischer, Gauger, & Sedlmayer (1995) examined some causes of instability not depending on the stellar pulsations that cause the dust to form periodically. The combination of the eigenperiod introduced by the instabilities with the period of stellar pulsations may lead to an effect of multiperiodicity of the dust formation with regard to the pulsation cycle. The multiperiodicity has effect both on the light curves and on the visibility curves (Winters et al. 1995). It is possible that such a mechanism could describe some of the phenomena associated with Mira. The dust shell expansion is less than 1 $R_*$ per cycle of luminosity (the terminal velocity of the CO envelop of Mira given by Knapp 1985 is 4 km $s^{-1}$). The multiple fronts of dust assumed in Clump3 models are separated by about 10 $R_*$ of distance. This is too large a distance to be locked only to the stellar pulsation and it is thus reasonable to think that the dust may form multiperiodically around Mira.

The formation of a new clump of dust may cause both the change observed in the 1992 visibility curve and some of the variations detected in the OH maser emission. Since 1990 November the Nançay radio telescope has been regularly used to monitor the activity of the OH masers (Gérard & Bourgois 1992). Different kinds of variations are observed. The year 1992 seems peculiar considering the following remarks (E. Gérard 1995a, 1995b, private communication):

1. The circular left-hand polarization component of the 1665 MHz emission has increased by a factor of 2.5 two months after the 1992 maximum light of Mira. The 1992, 1993, and 1994 maxima are identical. The maximum of 1995 is lower and comparable to those of 1990 and 1991.
2. A redshifted component of the 1665 MHz emission occurred in 1992. This emission was not observed in later runs.
3. A hyperfine transition at 1667 MHz has been detected only in 1992 October (two months after the visible maximum of Mira).

It is tempting to seek an explanation for visibility changes linked to the formation of new dust particles as suggested by our sequence of models. The 1665 MHz maser emission is known to be pumped by far-infrared radiation. An increase in far-infrared emission may be produced if new dust condenses in the inner region of the shell. The presence in 1992 of an optically thick additional clump of dust [models Clump1(b), Clump2(b) and Clump3(b)] agrees with this situation. Another consequence is that the temperature at the side of the optically thick clump away from the star is decreased. The 1667 MHz transition, which is supposed to be located between 10 and 40 AU from the star, is assumed to be sensitive to the temperature variation (E. Gérard 1995b, private communication). The presence of a large amount of newly condensed dust particles may produce large changes in the 1667 MHz emission because of the change of temperature.

Large amounts of dust may form during some peculiar maximum of luminosity such as the one of 1992. Monitoring of the dust shell is needed to get as much as information

as possible during such an event. Such maxima may occur every 3–4 cycles of the visible light curve. It is clear that more visibility observations are needed during minimum luminosity.

Although present measurements identify some of the complexities in behavior of o Cet, further observations will be required to more fully understand the origins of the dramatic changes observed in the visibility data. For example, better coverage of the ($u$, $v$) plane in a timescale short compared to the variation of the object will certainly be important. Such observations will be possible within the next 2 years after the present expansion of the ISI system is completed, which will then include three telescopes and hence will measure three baselines simultaneously as well as one closure phase. Measurement of the closure phase will be very helpful in the analysis of the symmetry of the object Fourier transform.

We thank P. Couteau, E. Gérard, and T. Lebertre for helpful discussion. The Association Française des Observateurs d'Etoiles Variables (AFOEV) light curves were kindly provided by E. Schweitzer. A portion of this work was supported by the France-Berkeley Fund, which provided for a 4 months postdoctoral grant for B. Lopez. We thank the French PNHRA "Programme National de haute Résolution Angulaire" and the GdR 968 "Milieux Circumstellaires" for travel grants. The United Kingdom Infrared Telescope is operated by the Joint Astronomy Centre on behalf of the UK Particle Physics and Research Council. Long baseline interferometry in the mid-infrared at U. C. Berkeley is supported by the National Science Foundation (grants AST 93-21384, AST 93-21289, & AST 95-00525) and by the Office of Naval Research (OCNR N00014-89-J-1583 & FDN0014-96-1-0737).

## REFERENCES

Bester, M., Danchi, W. C., Degiacomi, C. G., Greenhill, L. J., & Townes, C. H. 1992, ApJ, 392, 357
Bester, M., Danchi, W. C., Degiacomi, C. G., Townes, C. H., & Geballe, T. R. 1991, ApJ, 367, L27
Bester, M., Danchi, W. C., Hale, D., Townes, C. H., Degiacomi, C. G., Mekarnia, D., & Geballe, T. R. 1996, ApJ, 463, 336
Bester, M., Danchi, W. C., & Townes, C. H. 1990, Proc. SPIE, 237, 40
Bloemhof, E. E., Townes, C. H., & Van der Wyck, A. H. B. 1984, ApJ, 276, L21
Bowen, G. 1988, ApJ, 329, 299
Bujarrabal, V., Alcolea, J., & Planesas, P. 1992, A&A, 257, 701
Danchi, W. C., & Bester, M. 1995, Ap&SS, 224, 339
Danchi, W. C., Bester, M., Degiacomi, C. G., Greenhill, L. J., & Townes, C. H. 1994a, AJ, 107, 1469
Danchi, W. C., Bester, M., Degiacomi, C. G., & Townes, C. H. 1990, ApJ, 359, L59
Danchi, W. C., Bester, M., Greenhill, L. J., Degiacomi, C. G., & Townes, C. H. 1994b, Proc. SPIE, 2200, 286
Danchi, W. C., Degiacomi, C. G., Bester, M., Greenhill, L. J., & Gezari, D. Y. 1992, in ESO Conf. Proc. 39, High Resolution Imaging by Interferometry II, ed. J. M. Beckers & F. Merkle (Garching: ESO), 21
David, P., & Papoular, R. 1992, A&A, 265, 195
Degiacomi, C. G., Bester, M., Danchi, W. C., Greenhill, L. J., & Townes, C. H. 1992, in ESO Conf. Proc. 39, High Resolution Imaging by Interferometry II, ed. J. M. Beckers & F. Merkle (Garching: ESO), 681
Diamond, P. J., Kemball, A. J., Junor, W., Zensus, A., Benson, J., & Dhawan, A. 1994, ApJ, 430, L61
Draine, B. T., & Lee, H. M. 1984, ApJ, 285, 89
———. 1987, ApJ, 314, 485
Fleischer, A. J., Gauger, A., & Sedlmayer, E. 1995, A&A, 297, 543
Gérard, E. 1995a, Rencontre de Travail Miras, ed. M. O. Mennessier, 5
Gérard, E., & Bourgois, G. 1992, in Lecture Notes in Physics, Astrophysical Masers Conf., ed. A. W. Clegg & G. E. Nedoluha (Berlin: Springer), 365
Greenhill, L. J., Colomer, F., Moran, J. M., Backer, D. C., Danchi, W. C., & Bester, M. 1995, ApJ, 449, 365
Haniff, C., Ghez, A. M., Gorham, P. W., Kulkarni, S. R., Matthews, K., & Neugebauer, G. 1992, AJ, 103, 1662
Hearn, A. 1990, From Miras to PN: Which Path for Stellar Evolution? (Gif-sur-Yvette: Editions Frontiéres)
Iben, I. 1985, in Mass Loss from Red Giants, ed. M. Morris & B. Zuckerman (Dordrecht: Reidel), 1
———. 1991, ApJS, 76, 55
Karovska, M., Nisenson, P., & Beletic, J. 1993, ApJ, 402, L311
Karovska, M., Nisenson, P., Papaliolios, C., & Boyle, R. P. 1991, ApJ, 374, L51
Knapp, G. R. 1985, ApJ, 293, 273
Knapp, G. R., & Morris, M. 1985, ApJ, 292, 640
Lefèvre, J., Bergeat, J., & Daniel, J.-Y. 1982, A&A, 114, 341
Lockwood, G. W., & Wing, R. F. 1971, ApJ, 169, 63
Lopez, B., Mékarnia, D., & Lefèvre, J. 1994, A&A, 296, 752
Mathis, J. S., Rumpl, W., & Nordseick, K. H. 1977, ApJ, 217, 425
Meixner, M. 1993, Ph.D. thesis, Univ. California, Berkeley
Nishimoto, D., Kissell, K. E., Africano, J. L., Lambert, J. V., & Kervin, P. W. 1995, unpublished
Planesas, P., Kenney, & J.,Bachiller, R. 1990, ApJ, 364, L9
Press, W. H., Teukolsky, S. A., Vetterling, W. T., & Flannery, B. P. 1992, Numerical Recipes in C (2d ed.; New York: Cambridge Univ. Press)
Quirrenbach, A., Mozurkewich, D., Armstrong, J. T., Colavita, M. M., & Shao, M. 1992, A&A, 259, L19
Reimers, D., & Cassatella, A. 1985, ApJ, 297, 275
Rowan-Robinson, M., & Harris, S. 1983, MNRAS, 202, 767
Sahai, R., & Bieging, J. H. 1993, AJ, 105, 595
Tuthill, P. G. 1994, Ph.D. thesis Univ. Cambridge
Tuthill, P. G., Haniff, C. A., & Baldwin, J. 1995, MNRAS, 277, 1541
van der Veen, W. E. C. J., Omont, A., Habing, H. J., & Mathews, H. E. 1995, A&A, 295, 445
Wilson, R. W., Baldwin, J., Buscher, D. F., & Warner, P. J. 1992, MNRAS, 257, 369
Winters, J. M., Fleischer, A. J., Gauger, A., & Seldmayr, E. 1995, A&A, 302, 483
Wolfire, M. G., & Cassinelli, J. P. 1986, ApJ, 310, 207
Young, K. Y. 1995, ApJ, 445, 872